Australian Government
Geoscience Australia

Offshore Northern Perth Basin 2D and 3D Models of Depth to Magnetic Basement

Record
2012/39

GeoCat # 73002

Stephen Johnston and Peter Petkovic

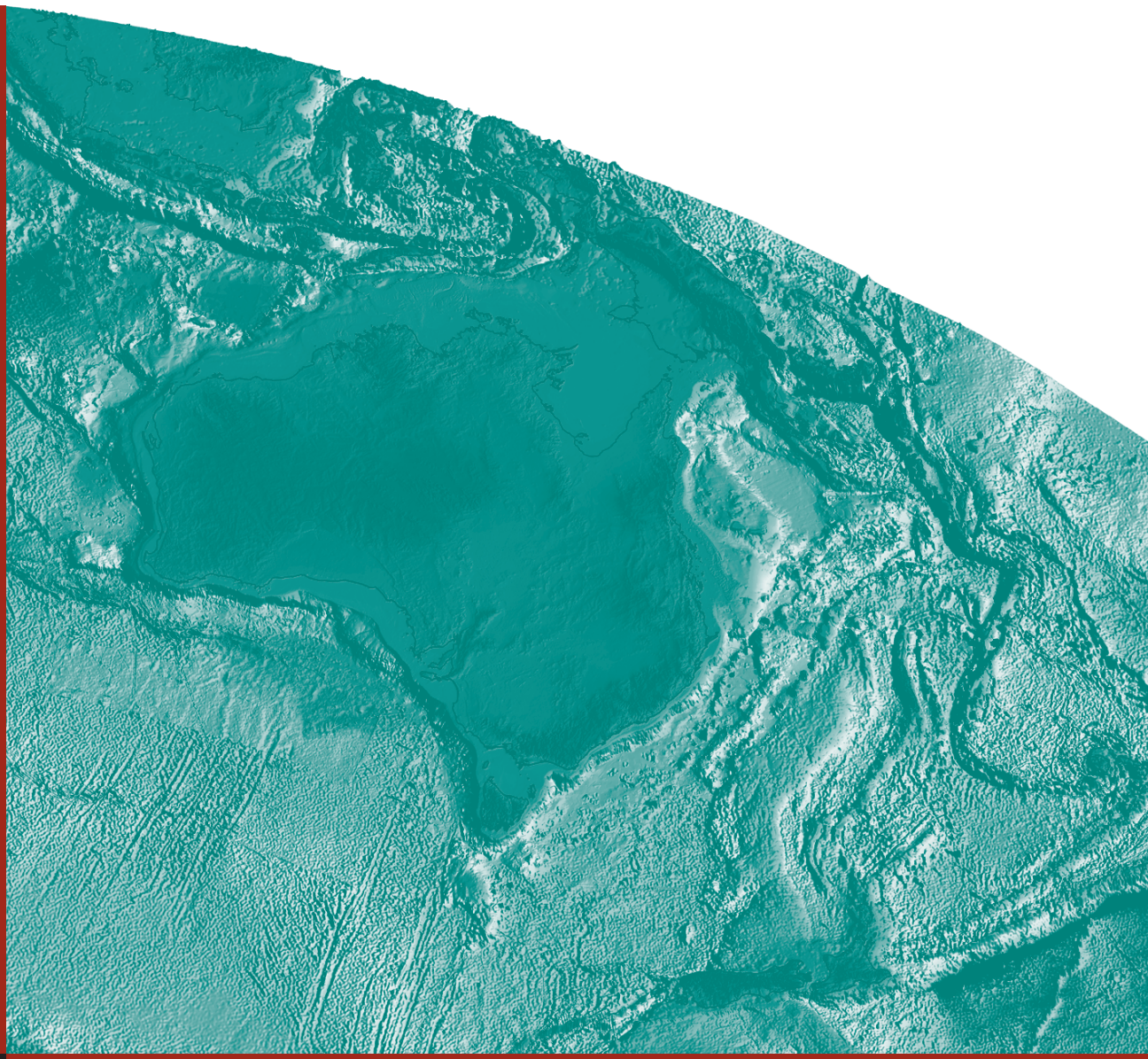

Offshore Northern Perth Basin 2D and 3D Models of Depth to Magnetic Basement

GEOSCIENCE AUSTRALIA
RECORD 2012/39

by

Stephen Johnston and Peter Petkovic

Australian Government
Geoscience Australia

Department of Resources, Energy and Tourism
Minister for Resources and Energy: The Hon. Martin Ferguson, AM MP
Secretary: Mr Drew Clarke

Geoscience Australia
Chief Executive Officer: Dr Chris Pigram

This paper is published with the permission of the CEO, Geoscience Australia

ISSN 1448-2177
ISBN 978-4-922103-22-2 (Web)
ISBN 978-4-922103-24-6 (CD)
ISBN 978-4-922103-23-9 (Hardcopy)

GeoCat # 73002

Bibliographic reference: Johnston, S. and Petkovic, P. 2012. Offshore Northern Perth Basin 2D and 3D Models of Depth to Magnetic Basement. Record 2012/39. Geoscience Australia: Canberra.

Contents

Executive Summary 1

Introduction 2

Observed Magnetic Data 3
- Susceptibility Measurements 3

Depth to Precambrian Basement 7
- Well Depths 7
- Onshore Depth Converted Seismic Interpretation of Precambrian Basement 7

2.5D Magnetic Models 8
- Profile A: A76a-24 10
- Profile B: GA310-31 + E92AU09-41R 12
- Profile C: GA310-29 17
- Profiles D and E: GA310-27 and B92-3509 22

3D Depth to Magnetic Basement Model 24
- Magnetic Spectral Depth to Sources Method 24
- Defining and Constraining Magnetic Basement 25
- Depth to Basement Grid 26
- Estimating Error in Basement Grid 29

Comparison between Magnetic Methods 30
- Profile A: A76A-24 30
- Profile B: GA310-31 + E92AU09-41R 30
- Profile C: GA310-29 31
- Profile D: GA310-27 31
- Profile E: B92-3509 31

Discussion and Conclusions 32

Acknowledgements 33

References 34

Appendix 1 – Magnetic susceptibility measurements 37

Appendix 2 – Comparison between depth to Precambrian from wells and power spectra 53

Executive Summary

During 2009-11 Geoscience Australia completed a petroleum prospectivity study of the offshore northern Perth Basin as part of the Australian Government's Offshore Energy Security Program and release of W11-18 acreage. A significant component of the program was the acquisition of a regional 2D reflection seismic and potential field survey GA-310 in 2008/09, which has aided in furthering the understanding of basement within the northern Perth Basin. Geologic basement in the northern Perth Basin, defined here to be Precambrian and older, is deep and generally not resolved in the reflection seismic data. However the GA-310 magnetic anomaly data combined with Geoscience Australia's magnetic ship-track database and magnetic anomaly grid allowed an assessment of depth to magnetic sources, and estimation of sediment thickness, providing new insight into basement depths and trends. New magnetic susceptibility measurements taken from core of offshore wells of the northern Perth Basin, seismic interpretation and depth to magnetic source estimates using the magnetic spectral method have been used to constrain 2.5D magnetic forward models. These magnetic models indicate that intrusion of the deepest sediments by high-susceptibility bodies is probable. The reflection seismic evidence for these bodies is not clear, though in some cases they may be associated with faults and structural highs. Where the modelled bodies penetrate the sediments they are mostly below or within the Permian strata. A moderate positive magnetic anomaly along the Turtle Dove Ridge is modelled in 2.5D by massive bodies whose tops are 5-15 km below sea floor. A depth to magnetic basement map highlights sub-basins and structural highs within the northern Perth Basin, and is shown to be a good first order approximation of sediment thickness and basin geometry. For instance, maximum sediment thicknesses of the Abrolhos, Zeewyck and Houtman sub-basins are shown to be 10, 13.5 and 12 km respectively.

Introduction

Sediment thickness is a fundamental parameter used to assess the petroleum prospectivity of a sedimentary basin. Therefore, mapping a basin's basement in terms of depth and structure is of primary importance. The northern Perth Basin is a sedimentary basin that has hydrocarbon discoveries both on and offshore; however the offshore remains largely under explored (Jones et al., 2011). Recent studies, however, indicate there is potential for new petroleum discoveries in many of these frontier areas (e.g. Nicholson et al., 2008; Borissova et al., 2010; Jones et al., 2011).

Despite the new geological insights gained from these studies, depth to basement beneath the offshore northern Perth Basin remains poorly understood. Conversely, in the onshore northern Perth Basin a number of wells intersect rocks of Precambrian age and seismic reflection data images the base of sediments (Mory and Iasky, 1996). Due to the thick sediments and high degree of structuring of the offshore northern Perth Basin seismic reflection data do not adequately resolve the geologic basement throughout most of the region. The deepest stratification observable in the reflection seismic data is interpreted to be Permian and older sediments (Jones et al., 2011; Nicholson and Bernardel, pers. comm.). The basement is thought to be Mesoproterozoic Pinjara Orogen high-grade metamorphic rock, outcropping onshore as the Northampton Block (Dentith et al., 1994; Hall, in prep) or Precambrian granites as sampled over the Beagle Ridge (Jones et al., 2011). Pre-rift sedimentary strata immediately overlying basement are likewise poorly understood and are speculated to be Late Cambrian to Ordovician sandstones, such as the Tumblagooda Sandstone which is interpreted in the Houtman Sub-Basin and Southern Carnarvon Basin (Iasky et al., 2003; Jones et al., 2011). In this study basement is defined to be the top of Precambrian geology.

Because of the difficulties in imaging the basement of the northern Perth Basin using seismic reflection data, magnetic data were used to map the depth to basement. Because the Precambrian geology contains magnetic minerals (Hall, in prep), magnetic data can be used to estimate the depth to Precambrian basement below the overlying sedimentary cover. Many methods exist for estimating depths from magnetic data (e.g. Gunn, 1997), but in this study 2.5D magnetic modelling and depth estimation using the magnetic spectral method (Spector and Grant, 1970) will be used to gain an understanding of the depth to basement in the northern Perth Basin,.

Magnetic bodies within the basin may represent various rock types, not all of which are defined as basement. For example, continental breakup in the Early Cretaceous (Valanginian) may have been accompanied by magmatic and volcanic activity (Symonds et al, 1998; Gorter and Deighton, 2002), resulting in emplacement of magnetic material throughout the sedimentary and basement section. Other volcanic episodes include a period of rifting during the early Jurassic (Jones et al., 2011). Evidence of other magnetic rocks include olivine and alkali basalts collected on marine survey GA-2476 in 2008 (Heap and Harris, 2008; Daniell et al., 2009) from the sea floor on slopes and canyons over Houtman and Zeewyck sub-basins, with a deep source suggested by the geochemistry (Dadd and Kellerson, 2011).

Because of the complex distribution of magnetic sources within the northern Perth Basin, care was taken to discriminate between shallow and basement related magnetic sources in the 2.5D forward models and in the depth to basement grid using the magnetic spectrum method. This was achieved by constraining the forward models and depth to basement results by gravity, seismic reflection and well data.

Observed Magnetic Data

In late 2008/09, as part of the Australian Government's Energy Security Program (2006–2011), Geoscience Australia acquired 26,000 line kilometres of new potential-field data (Foster et al., 2009). These new data were merged and levelled (Hackney and Morse, 2011; Hackney et al., 2012) with an existing Australia-wide dataset of levelled marine data (Petkovic et al., 2001) and subsequently combined with onshore data from the 5th Edition of the Magnetic Map of Australia (Milligan et al., 2010) and the 2010 release of the Australian National Gravity Database. The final compilation (shown in *Figure 1*) provides a consistent onshore/offshore dataset that covers the entire Southwest Margin of Australia, and is the primary dataset used for the magnetic spectrum modelling portion of this study.

Five 2.5D magnetic forward models were generated in this study from seismic lines GA310-27, 29 and 31, A76A-24 and E92Au09-41R (see below for more details). Magnetic data for modelling Geoscience Australia survey 310 lines were obtained from observed anomaly values recorded in the survey's navigation file, using Petrosys as an intermediary process to compute spatial coordinates of the magnetic measurements. The 2.5D model containing line GA310-31 was extended by line E92Au09-41R which had no magnetic data in the navigation file. For this latter portion the magnetic data were extracted from a grid of levelled line data by Hackney and Morse (2011), and levelled by applying a shift to match the end of GA310-31. The join was made at shot point 3746 on GA310-31 and shot point 1917 on E92Au09-41R, and shot numbering re-sequenced along the profile, and subsequently referred to as 'Profile B'. Magnetic data for profiles A (seismic line A76A-24) and E (seismic line B92-3509) were also derived from the grid of levelled data. A regional view of the magnetic anomaly data is given in the reduced-to-pole grid compiled from levelled ship-track data by Hackney and Morse (2011) (*Figure 1*).

SUSCEPTIBILITY MEASUREMENTS

For comparison to representative published values (discussed below), measurements were carried out on core and cuttings from offshore North Perth Basin wells using an Exploranium KT5 model magnetic susceptibility meter using the following procedure:

1. Calibrate the device against empty air.
2. Put the device in contact with a rock sample and take another reading; the change in emitted magnetic field caused by the presence of magnetic minerals in the sample is used to calculate the magnetic susceptibility of the rock sample.

The samples were held in contact with the device, whilst care was taken to keep the device away from metallic objects and electromagnetic fields during calibration and measurement. Up to five measurements were taken for every 50 cm interval of core, and an average taken for each interval. The measurements are given in Appendix 1.

A summary of the measurements is given in *Table 1* excluding 5% highest samples and 5% lowest from the mean and standard deviation. The mean of sedimentary rock samples across the seven wells ranges from 0.00003 to 0.00015 SI. In these wells the only igneous rock, a volcanic pebble noted in Houtman 1 well, was measured at 0.0009 SI. Basement susceptibilities range from 0.00008 to 0.00039 SI.

Table 1. ***Magnetic susceptibility measurements for the sedimentary and basement sections of selected wells (SI x 10^{-3}). TD is total depth (m), N is number of samples whose range of values is given in column RANGE. The average (MEAN) and standard deviation (SD) are for the entire set of magnetic susceptibility measurements in the median 80% of values.***

SEDIMENT

WELL	TD (m)	n	MEAN	SD	RANGE
Perseverance 1	1045	53	0.12	0.03	0.05-0.24
Edel 1	987	23	0.05	0.03	0.02-0.27
Cliff Head 4	1414	50	0.10	0.05	0.03-0.38
Cliff Head 6	1368	122	0.05	0.03	0.00-0.19
Batavia 1	2794	14	0.03	0.01	0.02-0.05
Gun Island 1	138	108	0.11	0.06	0.02-1.14
Houtman 1	3074	75	0.15	0.05	0.05-1.49

BASEMENT

WELL	TD (m)	n	MEAN	SD	RANGE
BMR 10A	1430	6	0.19	0.20	0.10-0.59
Jurien 1	1026	1	0.08	0.02	-
Sue 1	3074	1	0.39	0.32	-

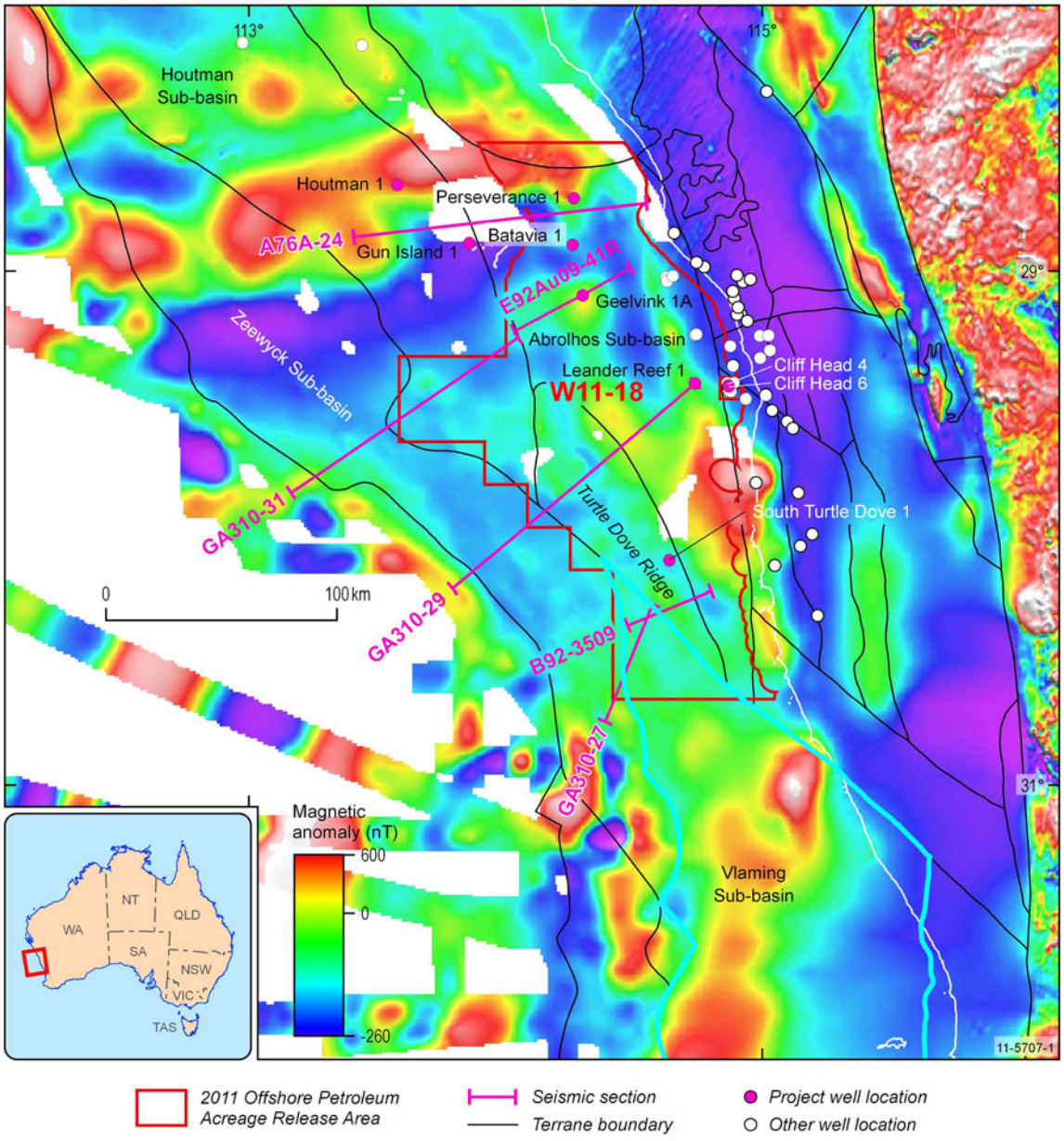

Figure 1. Location of study area in the northern Perth Basin showing seismic lines modelled, sub-basin and terrane boundaries (black) and acreage release area W11-18 (red). The base image is magnetic anomaly reduced-to-pole (Hackney and Morse, 2011). Onshore and offshore basement intersecting wells are also shown.

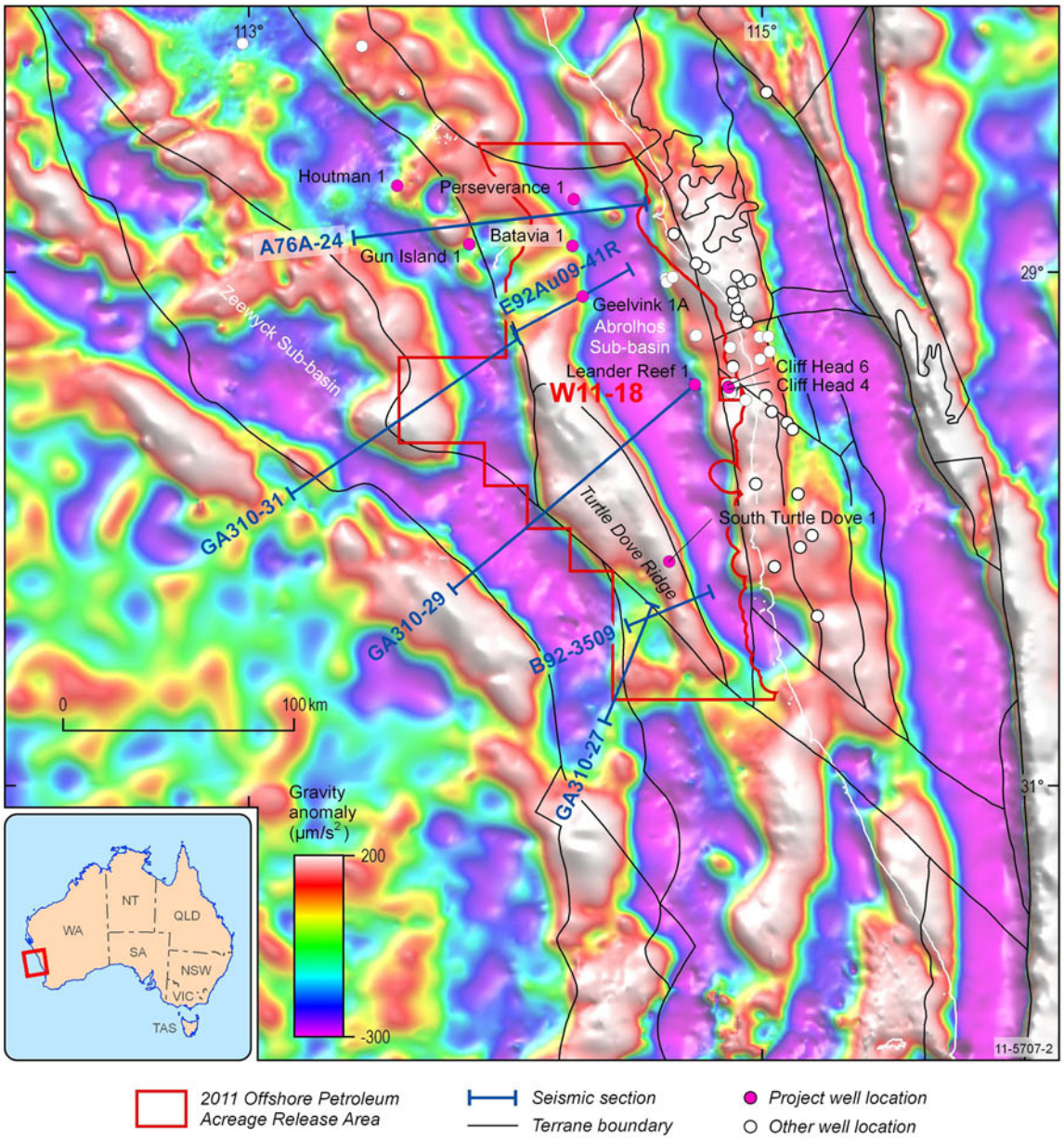

Figure 2. Location of study area in the northern Perth Basin showing seismic lines modelled, sub-basin boundaries (black) and acreage release area W11-18 (red). The base image is residual Bouguer gravity anomaly after subtraction of an upward continuation to 25km. (Hackney and Morse, 2011). Onshore and offshore basement intersecting wells are shown also.

Depth to Precambrian Basement

WELL DEPTHS

Depths to Precambrian geology from wells (*Table 2*) were obtained from Hall (in prep). These depths were used to calibrate magnetic power spectrum depths and to constrain the final depth to magnetic basement grid.

Table 2. ***Wells of the northern Perth Basin that intersect Precambrian basement. Depths are given in metres below surface topography. All are onshore except for Cliff Head 4 and 5 and Twin Lions 1. Well data was obtained from the Western Australian Petroleum and Geothermal Information Management System (http://www.dmp.wa.gov.au/4187.aspx).***

Well	Longitude	Latitude	Depth (m)
Arramall 1	115.0972	-29.5898	2188
Arrowsmith 1	115.1186	-29.6108	3363
BMR Beagle Ridge 10A	114.9750	-29.8267	1454
Beharra 1	115.0140	-29.4849	2013
Bonnifield 1	114.9145	-29.1703	991
Bookara 1	114.7731	-28.9835	242
Bookara 3	114.8903	-29.1074	442
Cadda 1	115.2148	-30.3363	2661
Cliff Head 4	114.8674	-29.4461	1562
Cliff Head 5	114.8781	-29.4698	1473
Conder 1	114.9242	-29.0440	200
Connolly 1 (Doral)	114.9531	-29.0365	338
Dongara 6	114.9411	-29.1948	1515
Eleven Mile 1	114.8839	-29.0763	270
Gairdner 1	115.1472	-30.0701	1990
Greenough 1	114.6565	-28.8528	428
Hampton Arms 1	114.7441	-28.9683	429
Jurien 1	115.0483	-30.1456	965
Mentelle 1	114.8892	-29.4359	1477
Rakrani 1	114.9012	-29.1702	1189
Robb 1	115.0383	-29.5453	1940
Twin Lions 1	114.8865	-29.3695	1513
Wakeford 1	114.9009	-29.0140	23
Wattle Grove 1	114.9064	-29.1429	762
Wendy 1	115.0167	-28.2991	1390
Woodada 19	115.1395	-29.8629	2795
Woolmulla 1	115.1942	-30.0232	2652
Woodleigh 1981/2	114.6686	-26.0548	171

ONSHORE DEPTH CONVERTED SEISMIC INTERPRETATION OF PRECAMBRIAN BASEMENT

Onshore interpretation of depth to basement from seismic data was taken from Mory and Iasky (1996) and is integrated into the final depth to basement grid (*Figure 18*).

2.5D Magnetic Models

Five transects were investigated by 2.5D magnetic forward modelling. These transects are shown in *Figures 1 and 2* with their survey and line name, with identifiers given in Table 3.

Table 3. Model profile identifiers and coincident seismic line names and lengths.

PROFILE	SEISMIC LINE NAME	LENGTH (KM)
A	A76A-24	106
B	GA310_31 + E92Au09-41R	153
C	GA310_29	125
D	GA310_27	52
E	B92-3509	33

Interpretations of these reflection seismic lines, and most of the others in the study area, do not include a basement horizon (C. Nicholson and G. Bernardel, pers. comm.). In lieu of this, an image of depth converted horizons (*Table 4*) was used to guide the modelling.

Table 4. ***Horizons mapped in Geoframe™ project (Nicholson and Bernardel, pers. comm.). 'NAME' is the code used in the GeoFrame™ interpretation project.***

NAME	DESCRIPTION
Wb	Water bottom
a_Val	Valanginian regional breakup unconformity
a_Yarragadee_SB	Base Yarragadee SB
a_lPerm	Late Permian regional unconformity
a_Perm_base	Base Early-Mid Permian syn-rift section
base_sect_resol	Base of resolvable section, i.e. visibility limit for interpretation of geology (denoted by 'BRS' in figures)
Moho	Undefined

The conversion of interpreted horizon TWT to metric depth was achieved using Petrosys software with average velocity of each horizon computed from uncorrected stacking velocities. The horizons were imported into a Petrosys project by direct link to Geoframe™. No attempt was made to calibrate the stacking velocities against interval velocities measured in wells (e.g. Johnston and Goncharov, 2012.) for the purpose of guiding the 2.5D modelling, because of the uncertainty of calibration below well depths (e,g. those presented in *Table 2*), and the sparse distribution of well data.

The strategy for building the 2.5D models was firstly to assume a magnetic basement of metamorphic rock below the horizon 'base_sect_resol' (BRS in the 2D figures). This deep body was extended ±100 km in-line beyond the data coverage to avoid end of line effects. The bodies were assumed to be a polygonal prism extending 500 km perpendicular to the plane of each section which was large enough for the 2.5D models to be considered effectively 2D. The bottom surface of this body was placed horizontally at approximately 30 km below sea level. The top surface was initially placed close to, and below 'base_sect_resol' (BRS), to model as much as possible the long wavelengths in the observed field.

A magnetic susceptibility of 0.02 SI was found to give a reasonable degree of long-wavelength fit to the observed data, however, this value is at the high end of Clark (1999) and Telford et al. (1976) estimates (*Table 5*). No known susceptibility measurements were available at the time of writing for the nearest outcropping basement rocks, those of the Northampton Block to the northeast, presumed to be equivalents of the study area basement rocks. Basement was penetrated in three onshore wells (*Table 1*) with susceptibilities averaging 0.0002, which is near the extreme low end of ranges given by Carmichael (1989) and Clark (1999). Our chosen value of 0.002 SI was deemed a suitable compromise, though arbitrary estimate, for the metasedimentary/metaigneous rocks assumed to

constitute the basement in the study area. Granite assemblages were not considered for modelling, having susceptibilities as low as 0.00001 SI or, if magnetite bearing, 0.001 – 0.01 SI (Gregorova et al., 2003). No attempt was made to model the effects of remnant magnetisation which is considered a minor component.

Table 5. ***Magnetic susceptibility (SI) of igneous, metamorphic and sedimentary rocks. The values listed for Schmidt (2010) are derived from five sedimentary and one basalt sample from the Houtman sub-basin, and one basalt sample from the Zeewyck sub-basin.***

REFERENCE	MAFIC IGNEOUS	METAMORPHIC	SEDIMENTARY
Clark (1999)	0.005 – 0.06	0.0002 – 0.001, 0.004 – 0.03	10^{-5} -10^{-3}
Lindsley et al. (1966)	55%, 0.001-0.05	71% <0.001	73% <0.001
Carmichael (1989)	0.00025 – 0.06	0.00025 – 0.0025 metasediments 0.0025 – 0.05 metaigneous	0.00004 – 0.004
Telford et al. (1976)	0.00055 – 0.12 (av. 0.03)	0 – 0.07 (av. 0.004)	0 – 0.05 (av. 0.0009)
Schmidt (2010)	0.01-0.02	-	0.0008
North Perth (Appendix 1)	-	0.00008-0.00059	0-0.00149
North Perth Models	0.03-0.06	0.002	0

With basement having an assumed susceptibility of 0.002 SI it was not possible to model the higher frequency components of the observed field by simply varying the depth to the top of basement. In order to model the higher frequency components of the observed field, bodies were introduced near the top of the basement body using susceptibilities for mafic igneous rock within the ranges noted in *Table 5*. Both dyke and sill shaped bodies were tested and found to produce magnetic responses that fit the range of observed anomalies equally well. However, such bodies were not resolved in the sedimentary parts of the reflection seismic data, providing no geologically plausible scenarios that can be tested.

In view of this, and so as not to prejudice the geologic interpretation, we decided to model bodies of arbitrary shape, regardless of their geological likelihood, to produce the closest possible fit between computed and observed fields. We present two sets of these models, one with deep and an alternative with shallow placement of magnetic bodies. We provide pointers to where the shallow set of bodies would be located in the two-way travel time (TWT) domain of the reflection seismic data along the model profiles.

Encom's *ModelVision*™ v10 was used for the modelling. This software computes the potential field response of the user's model along a profile. The program's design favours modelling of environments in which discrete bodies are embedded in a country rock. The program is flexible enough to allow creation of basin style models in simple 2.5D (in which a finite strike length is assumed perpendicular to the profile).

The profiles modelled in this study coincide with reflection seismic lines described by Jones et al. (2011) through acreage release area W11-18 (*Figure 4* and *Figure 16*). The following section is a discussion and description of each of these transects, showing magnetic susceptibility profiles for 'deep' and 'shallow' versions together with reflection seismic sections for each profile indicating the

approximate location of inferred magnetic bodies from the 'shallow' version. In general, the modelled magnetic bodies are either too deep to be imaged or not visible in the reflection seismic data. For that reason, the bodies were given quasi-geological geometries aiming to minimise the misfit between observed and computed magnetic field. For that reason, the magnitude of the misfits given in *Table 6* should not be interpreted as giving preference to one set of models over another. Initial susceptibility values were assigned, then model geometries and susceptibility values heuristically altered to minimise the misfit. Finally, portions of model geometries coinciding with major anomalies were fine-tuned by allowing them to move under inversion.

After the 2.5D magnetic models were finalised the depth to magnetic basement grid derived by the spectral method, developed independently, was projected onto each transect, to allow comparisons between the two methods.

Table 6. ***RMS misfit between computed and observed magnetic anomaly for each of the profiles A-E for 'shallow' and 'deep' versions, for reference.***

PROFILE: LINE	'SHALLOW'	'DEEP'
A: A76A-24	1.6	1.4
B: GA310_31 + E92Au09-41R	1.7	1.4
C: GA310_29	1.7	1.9
C: GA310_29 (3D)	-	1.3
D: GA310_27	1.4	1.3
E: B92-3509	-	1.0

PROFILE A: A76A-24

The profile model along reflection seismic line A76A-24, acquired as a part of a marine seismic survey by Esso in 1976 (*Figure 4*), is an east-west trending line 105.8 km long extending from offshore near Geraldton and crossing the Abrolhos and Houtman sub-basins (*Figure 1* and *Figure 2*). The line passes south of wells Perseverance 1 and Houtman 1 and north of Batavia 1 and Gun Island 1 and crosses the northern-most part of the acreage release area W11-18 (Jones et al., 2011).

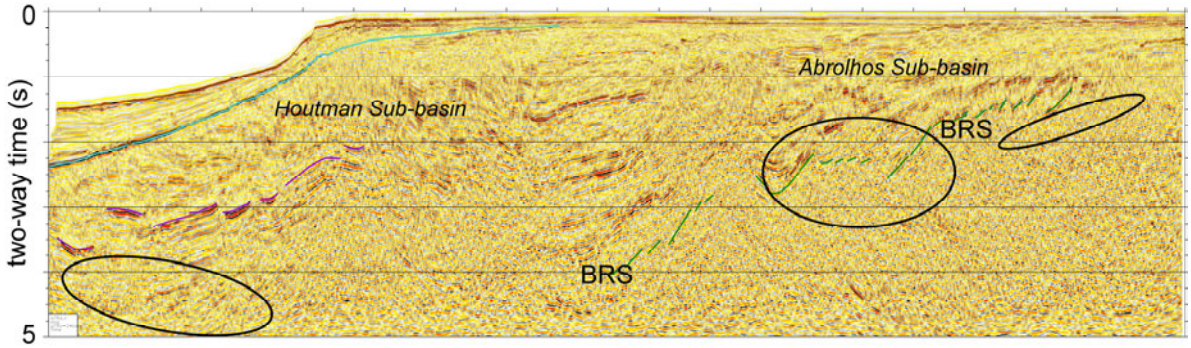

Figure 3. Reflection seismic data for line A76A-24 along Profile A showing 0-5 s TWT and 106 km line length. The ellipses indicate regions where magnetic bodies are modelled in the previous figure. 'BRS' is 'base of resolvable section', which is an approximate limit to the depth that sedimentary layering and structure can be inferred on the basis of seismic data.

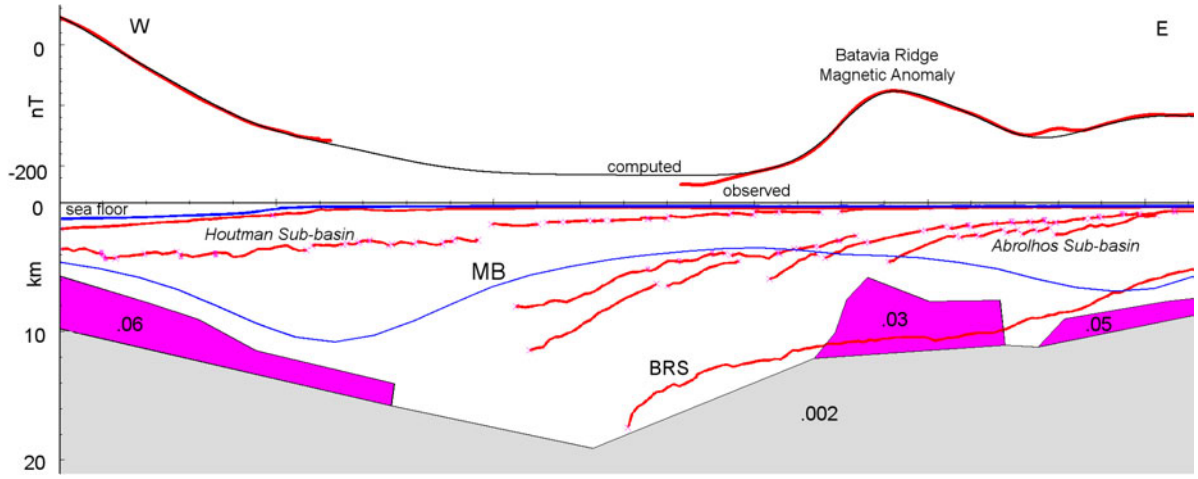

Figure 4. Profile A magnetic susceptibility model, 'shallow' version, along seismic line A76A-24 showing magnetic anomaly (upper) and depth section (lower). Line length is 106 km; V/H~1. The 'Batavia Ridge' magnetic anomaly is intersected as the prominent anomaly at the eastern end of this line. Magnetic susceptibilities are given in SI units. The anomaly is modelled by a large body emplaced above the limit of seismic reflectivity (BRS). Magnetic basement calculated using the spectral method is shown in blue (MB).

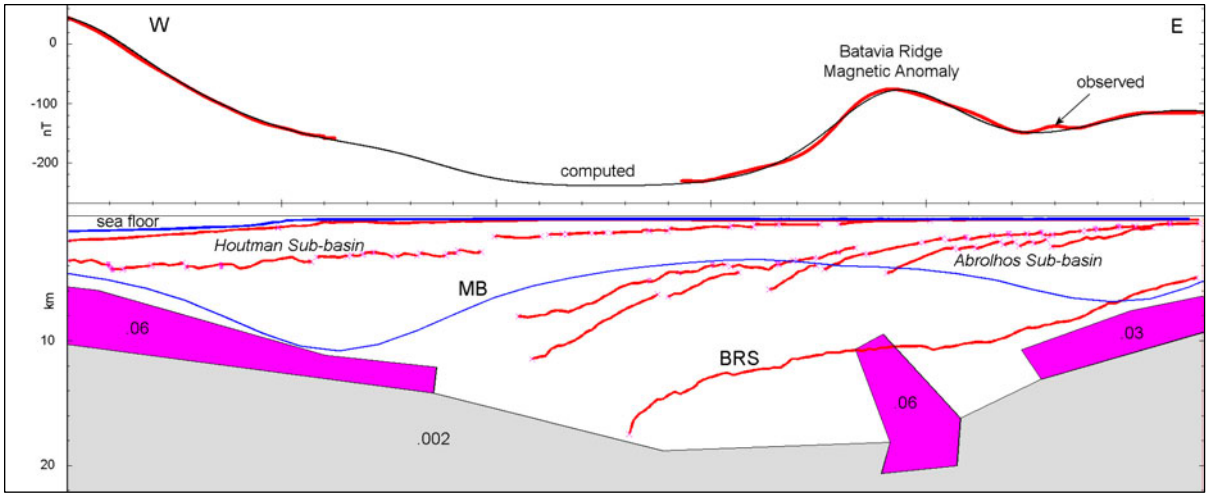

Figure 5. Profile A magnetic susceptibility model, 'deep' version, along line a76a-24 showing a deeper placement of a more highly magnetised modelled source of the 'Batavia Ridge' magnetic anomaly.

The eastern end of this line is covered by the southern part of the Rita marine seismic survey which is tied to Batavia 1[1]. The report on this survey (Roc Oil Pty Ltd, 2003) notes a deterioration of reflection seismic data quality in the Permian section of sandstones north of Batavia 1 speculating intrusions as the cause rather than data processing issues. This conclusion is supported by interpretation of volcanic plugs, sills, dykes and flows that form the Batavia Ridge magnetic anomaly crossed by Profile A (Gunn et al., 2004). The high magnetic susceptibility bodies (*Figure 4* and *Figure 5*) modelled near and below the limit of resolvable seismic section (between 5-20 km depth) may, therefore, be due to mafic intrusions that occur higher in the section. The 'shallow' option (*Figure 4*) uses a body of susceptibility 0.03 SI while the 'deep' option (*Figure 5*) is modelled by a narrower body of susceptibility 0.06 SI. In the region to the north of Profile A Gunn et al.

[1] Batavia 1 was drilled by Esso in 1978 and finished at 2941 m in Permian sandstone.

(2004) modelled magnetic basement depths at about 3-5 km using the Euler method supporting our 'shallow' interpretation.

The reflection seismic data show a highly faulted and chaotic reflectivity pattern at the two-way travel times corresponding to the depths to top of magnetic bodies modelled in this region (*Figure 3*), below which no clear geological structure can be inferred.

A magnetic basement of susceptibility 0.002 SI is interpreted as a broad trough in the centre of the line, although there is a gap in data in this region north of the Gun Island 1 well. The magnetic basement shallows towards the east in the direction of the metamorphic Northampton Block outcropping onshore north of Geraldton.

Westwards of the central trough the magnetic basement becomes shallower towards the oceanic crust and the broad positive anomaly at the western end of the line. The magnetic response of a thick dipping body of susceptibility 0.06 SI and 5-12 km deep models the observed magnetic data.

PROFILE B: GA310-31 + E92AU09-41R

Profile B trends NE-SW across the Abrolhos, Houtman and Zeewick sub-basins, passing through the Geelvink 1A[2] well. The profile is composed in its western part of Geoscience Australia marine survey line GA310-31 and in the east the "Plum" marine seismic survey line E92Au09-41R (Enterprise Oil, 1993a). This composite reflection seismic line is described by Jones et al. (2011) as a characteristic transect of acreage release area W11-18.

The models along this profile (*Figure 6* and *Figure 8*) include an undulating magnetic basement at 10-15 km depth. The magnetic basement follows the general trend of the 'base_sect_resol' or 'BRS' pseudo-horizon taken as the shallowest limit of basement. This topography and susceptibility of 0.002 SI accounts for only about ±5 nT variation in the model field. Several shallower more magnetically susceptible bodies are included in order to model the higher frequency anomalies.

An aeromagnetic survey covering the Abrolhos sub-basin section was flown in 1992 between 28°50'S and 29°35'S to the longitude of Gunn Island 1 well in the northwest corner of this survey. Enterprise Oil (1993b) interpreted the presence of magnetic source depths located from the near surface to 8 km, with magnetic basement deepening to the west.

The eastern part of the profile, seismic line E92Au09-41R shows economic basement less than 0.5 s TWT below the bottom of Geelvink 1A finishing in Triassic or Permian sandstones at 3053 m depth (Geelvink High, located near the peak of the large positive anomaly). The reflection seismic data do not conclusively show that this is top of basement and the preferred seismic interpretation (Nicholson and Bernardel, pers. comm.) is to place it deeper near 'base resolvable section' (BRS). However our magnetic modelling ('shallow' version, *Figure 6*) requires that the top of a large body with high magnetic susceptibility of 0.05 SI exists above BRS to model the prominent positive magnetic anomaly in this region. An equally good fit of observed and computed magnetic field can be achieved with a deeper placement and higher susceptibility (*Figure 8*) for the body below Geelvink 1A.

The anomaly which has a peak near Geelvink 1A may be a continuation of the Batavia Ridge magnetic anomaly noted by Gunn et al. (2004) and intersected in Profile A, although there is a magnetic trough between Geelvink 1A and Batavia 1 which is 40 km to the north (*Figure 1*).

[2] Geelvink 1 well was drilled by WAPET in 1978 and finished in Permian sandstone at 3053m.

Several large bodies are modelled to the west of Geelvink 1A, penetrating the base resolvable section in both 'deep' and 'shallow' versions and with depth to their tops of approximately 10 km (*Figure 6*). One such body is modelled dipping to the west, approximately coinciding with the Houtman Fault Zone (Figure 7, Jones et al., 2011) which may have provided a conduit for intrusion by deep-seated magmatic sources, or precipitation of magnetic minerals from fluid flow.

The fit between observed and modelled magnetic field is good everywhere along the line except minor differences at the eastern-most end of the profile where the profile enters a deep magnetic trough trending slightly west of north (*Figure 1*). This trough terminates beyond the profile in a positive north trending magnetic anomaly within the Abrolhos Sub-basin, and the source of this off-line anomaly is modelled approximately but not shown in the figures.

.

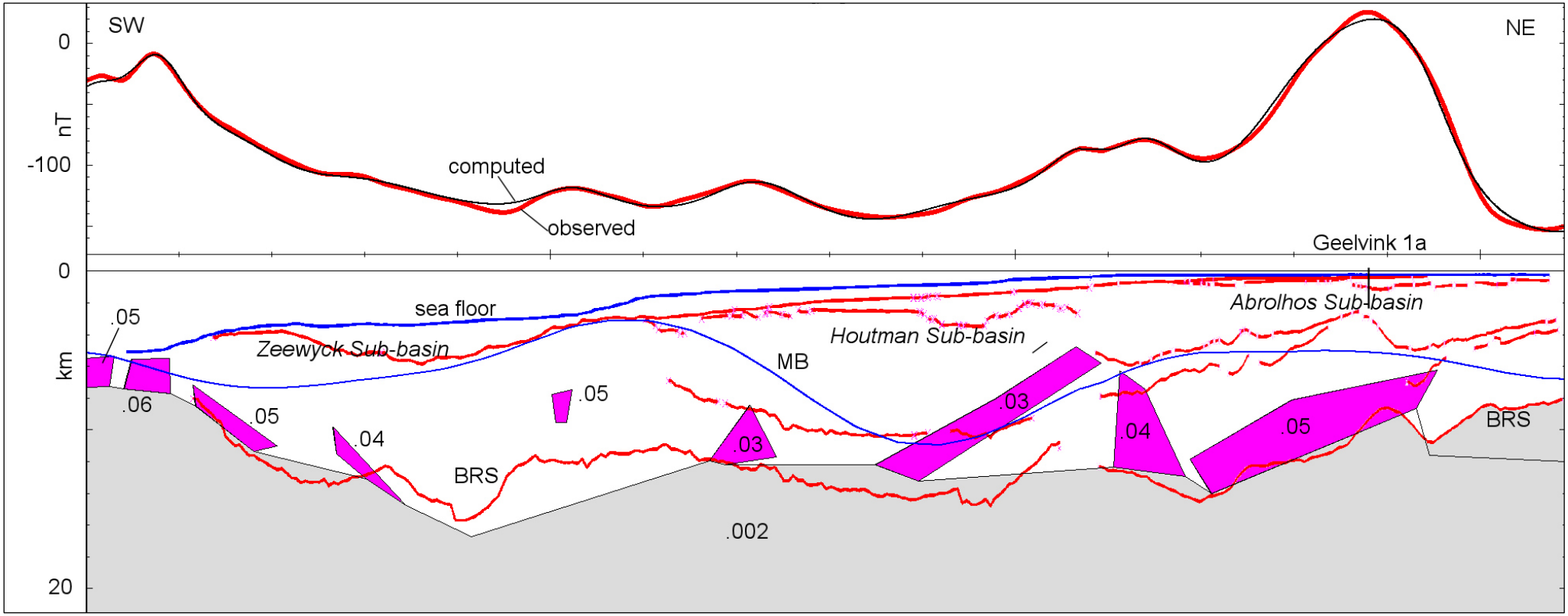

Figure 6. Profile B magnetic susceptibility model, 'shallow' version along seismic lines GA310-31 and E92Au09-41R showing magnetic anomaly (upper) and depth section (lower). V:H~1. 'BRS' is 'base resolvable section'. From west to east the line crosses the Zeewick, Houtman and Abrolhos Sub-basins. The prominent magnetic anomaly in the east appears to be a continuation of the "Batavia Ridge" magnetic anomaly (Gunn **et al.**, *2004). 'MB' is depth to magnetic basement determined from the power spectrum method; Zeewyck, Houtman and Abrolhos Sub-basins are indicated.*

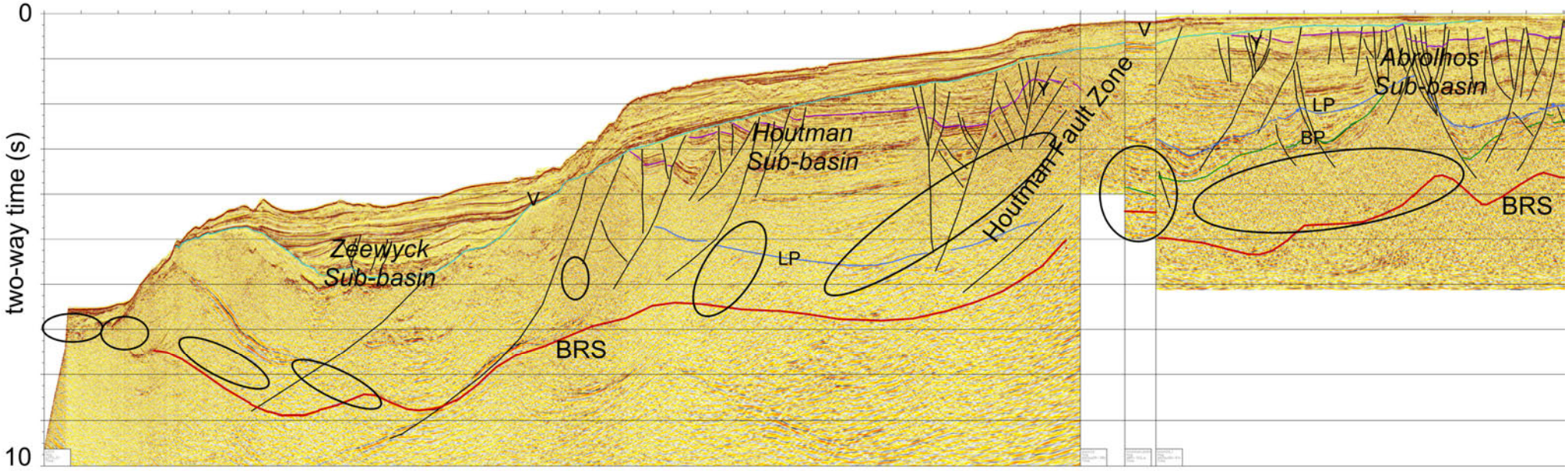

Figure 7. Seismic composite of lines GA310-31 and E92Au09-41R, along Profile B showing 0-10s TWT and 153 km line length. 'BRS' is 'base resolvable section'; 'BP' is base Permian; 'LP' is lower Permian; 'Y' is Yarragadee; 'V' is Valanginian breakup unconformity. The ellipses indicate regions where magnetic bodies are modelled in the previous figure.

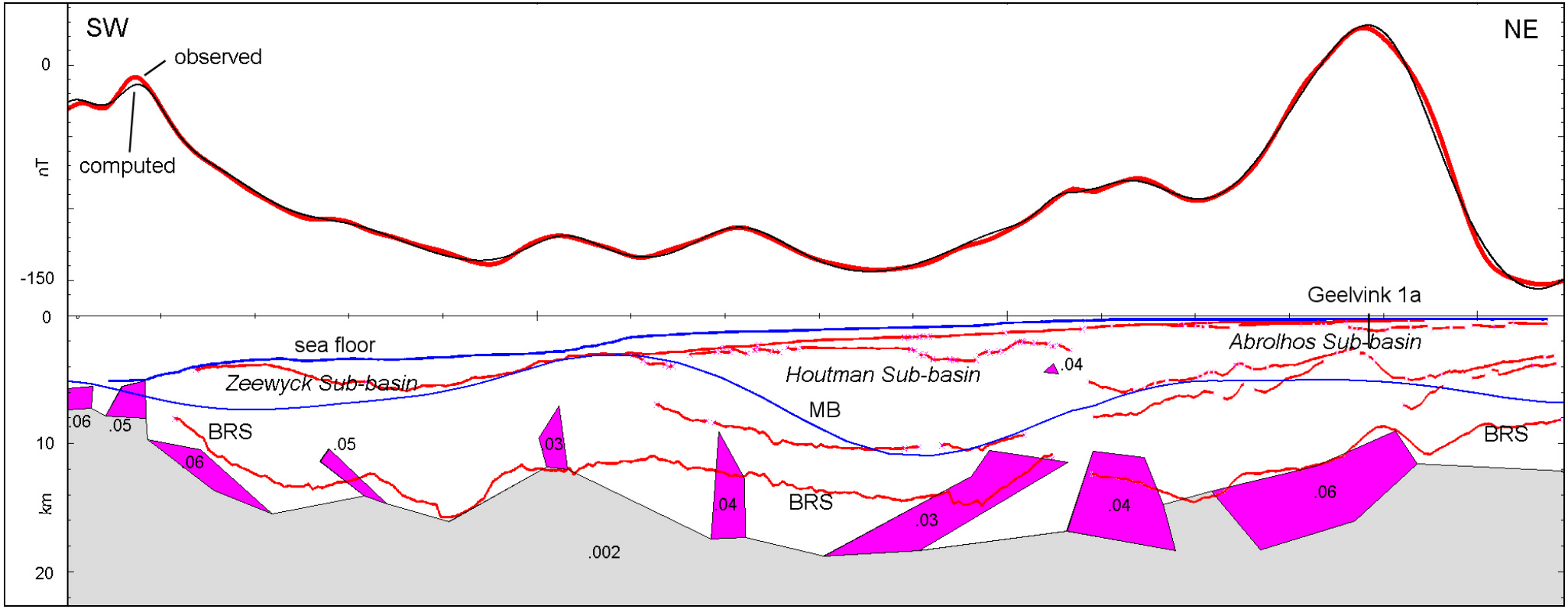

Figure 8. Profile B, 'deep' version: magnetic susceptibility model along lines GA310-31 and E92Au09-41R showing deeper placement of the modelled sources.

PROFILE C: GA310-29

Profile C is along reflection seismic line GA310-29 which trends NE-SW across the Abrolhos and Zeewyck Sub-basins and the Turtle Dove Ridge. The landward end ties to Leander Reef 1[3] well. Several complex 2D bodies were placed in the model to account for the observed magnetic anomalies. This reflection seismic line is described and interpreted by Jones *et al*. (2011) as a characteristic transect through acreage release area W11-18.

There is a large positive anomaly over the eastern half of the profile, over the boundary between the Turtle Dove Ridge and Abrolhos Sub-basin. This anomaly trends NNW (*Figure 1*) and is along the same N-S trend as the Batavia Ridge magnetic anomaly encountered on the two northern profiles. A large magnetically susceptible dipping slab can be placed at 5-10 km depth in both the 'shallow' (*Figure 9*) and 'deep' (*Figure 11* and *Figure 12*) variations to model this anomaly. The 'shallow' version places the top of this body above the base of resolvable reflection seismic section (BRS), while in the 'deep' version the top of the body is at approximately the same depth as the BRS.

A lesser anomaly marks the western boundary of the Turtle Dove Ridge, sufficiently modelled as vertical dykes in both 'deep' and 'shallow' versions to a depth of 5 km. By comparison, Jones (1983) estimated a depth to magnetic basement of 5-7 km in this area from contours of magnetic data acquired during a 2D reflection seismic survey by Ocelot International Pty. Ltd.

Other bodies are also modelled as penetrating the base of resolvable section to within 10 or 15 km of the surface. These bodies are not resolved in the reflection seismic data, though the fault system beneath the Turtle Dove Ridge may be associated with the large magnetic body modelled in this region (*Figure 10*). The western-most body is off-line (not shown), penetrates to near the sea floor and requires a significantly higher susceptibility to model the observed magnetic anomaly in this region. This body is located at the boundary of oceanic crust and is likely to be of mafic oceanic character. It is modelled with a susceptibility of 0.06 SI, less than the maximum of 0.1 SI listed by Carmichael (1989) for basalt samples.

Profile C intersects several linear magnetic anomalies obliquely (*Figure 1*). Orientations and inferred strike extent were used to modify the eastern half of the 'deep' 2D model of *Figure 11* to create what we refer to as a hybrid 3D model (*Figure 12*). The bodies in the eastern half of this figure do not have strike perpendicular to the profile.

[3] Leander Reef 1 well was drilled by Diamond Shamrock Oil in 1983 and finished in Lower Permian sediments at 3234m

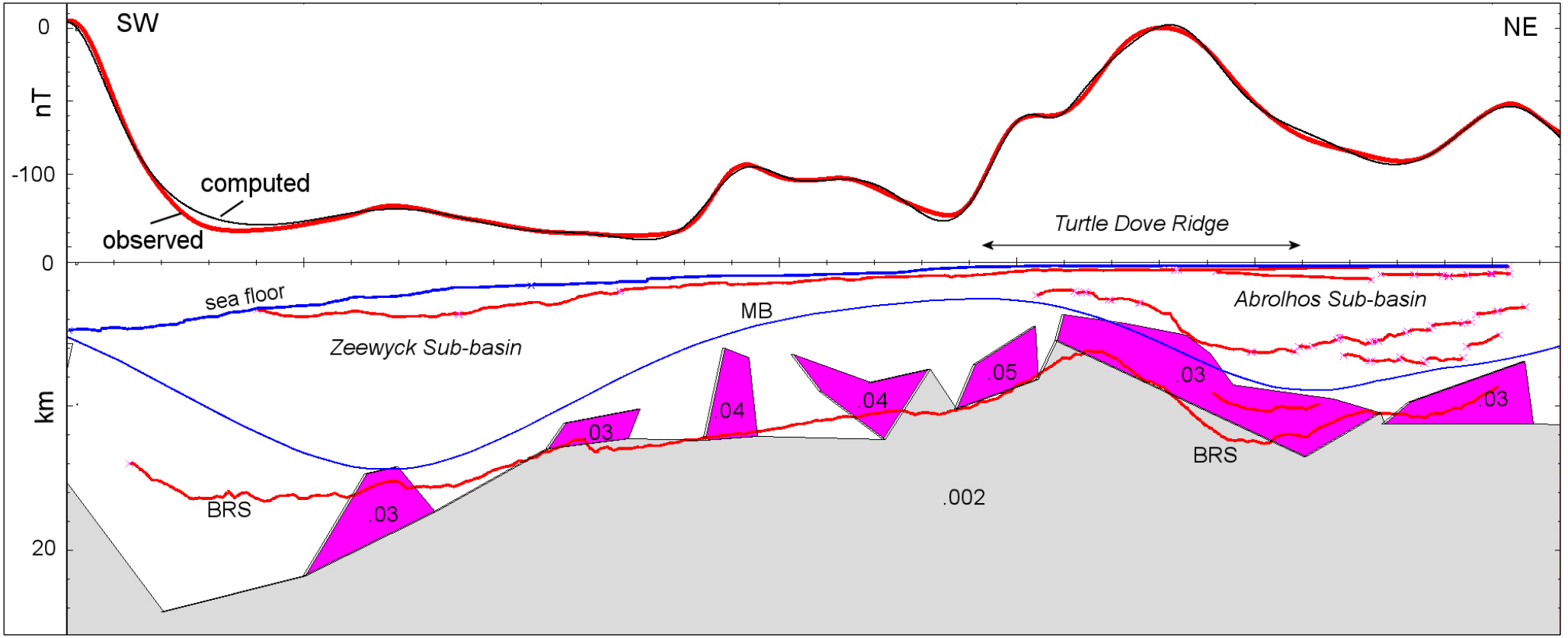

Figure 9. Profile C, 'shallow' version: magnetic susceptibility model along seismic line GA310-29 showing magnetic anomaly (upper) and depth section (lower).V:H~1. 'BRS' is 'base resolvable section'. The prominent positive anomaly above the Turtle Dove Ridge is modelled by a magnetic basement high topped by a slab of higher susceptibility material. 'MB' is top of magnetic basement determined from the power spectrum method.

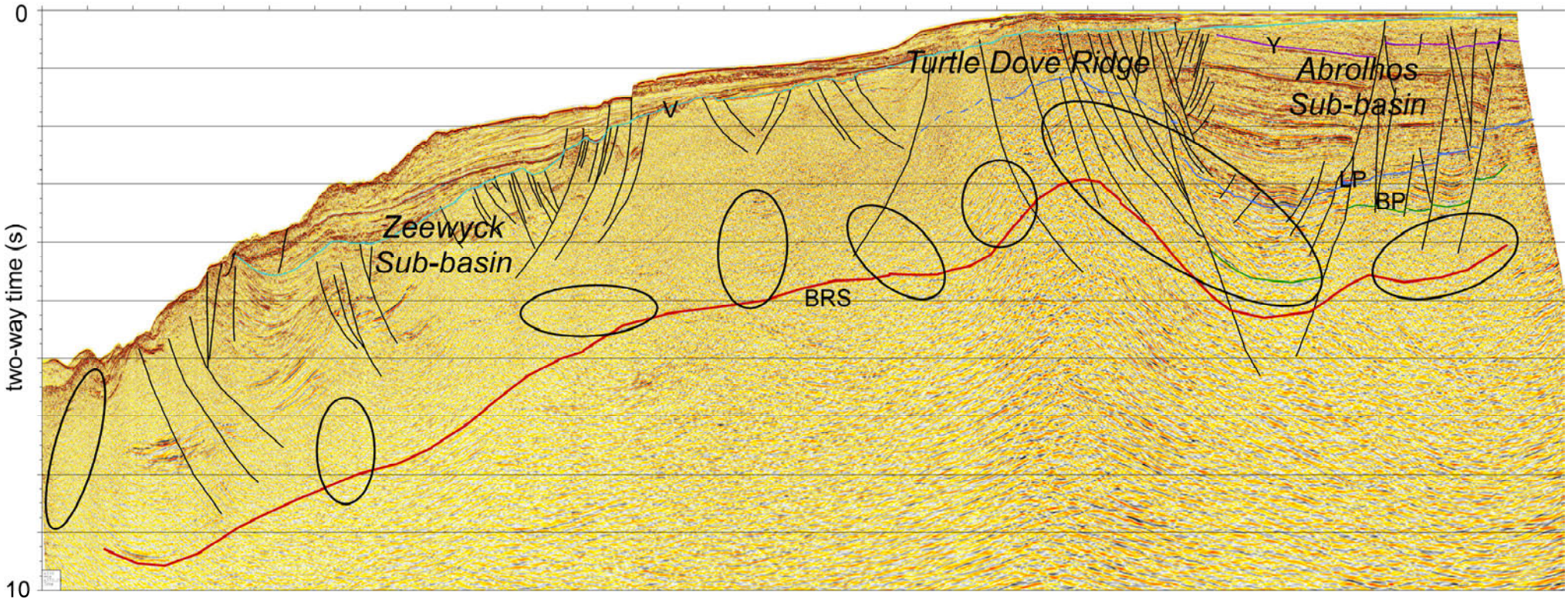

Figure 10. Profile C reflection seismic data for line GA310-29 showing 0-10s TWT and 125 km line length. Ellipses denote regions where magnetic bodies are modelled. 'BRS' is 'base resolvable section'; 'BP' is base Permian syn-rift section; 'P' is mid-Permian unconformity; 'Y' is base Yarragadee formation; 'V' is Valanginian unconformity.

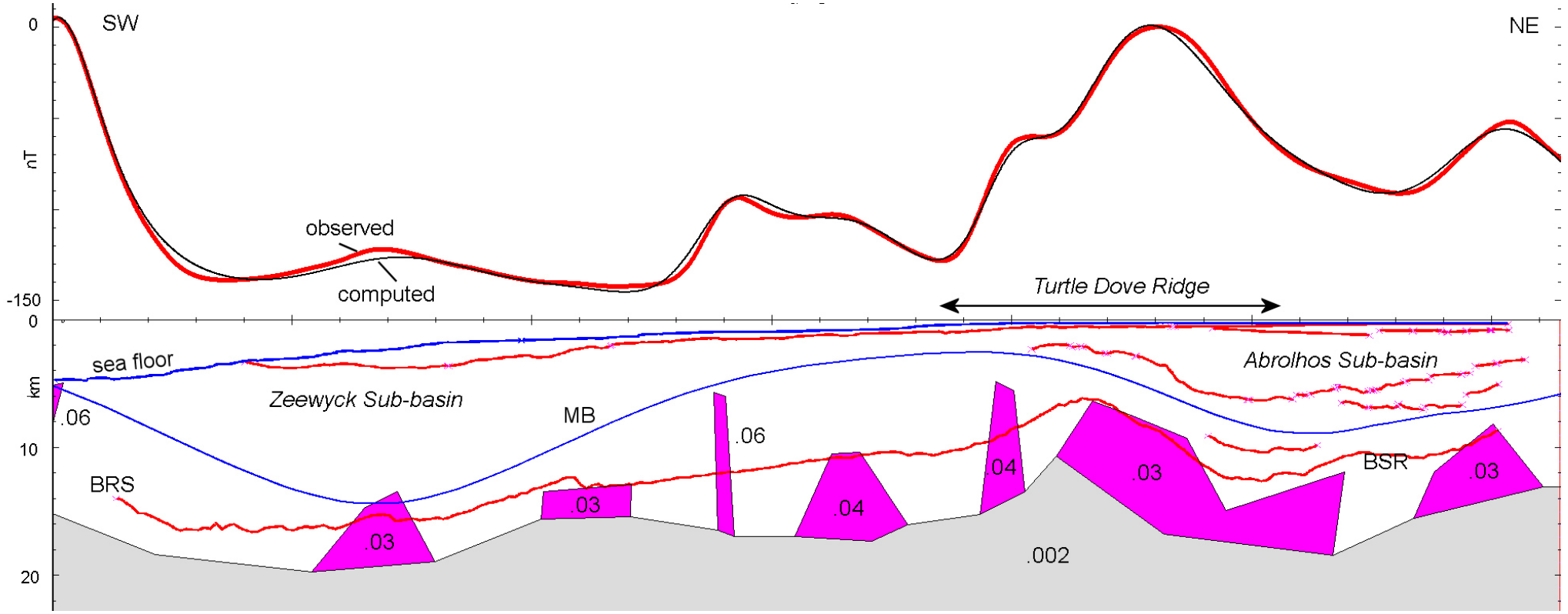

Figure 11. ***Profile C 'deep' version: magnetic susceptibility model along line GA310-29 showing deeper placement of the modelled sources.***

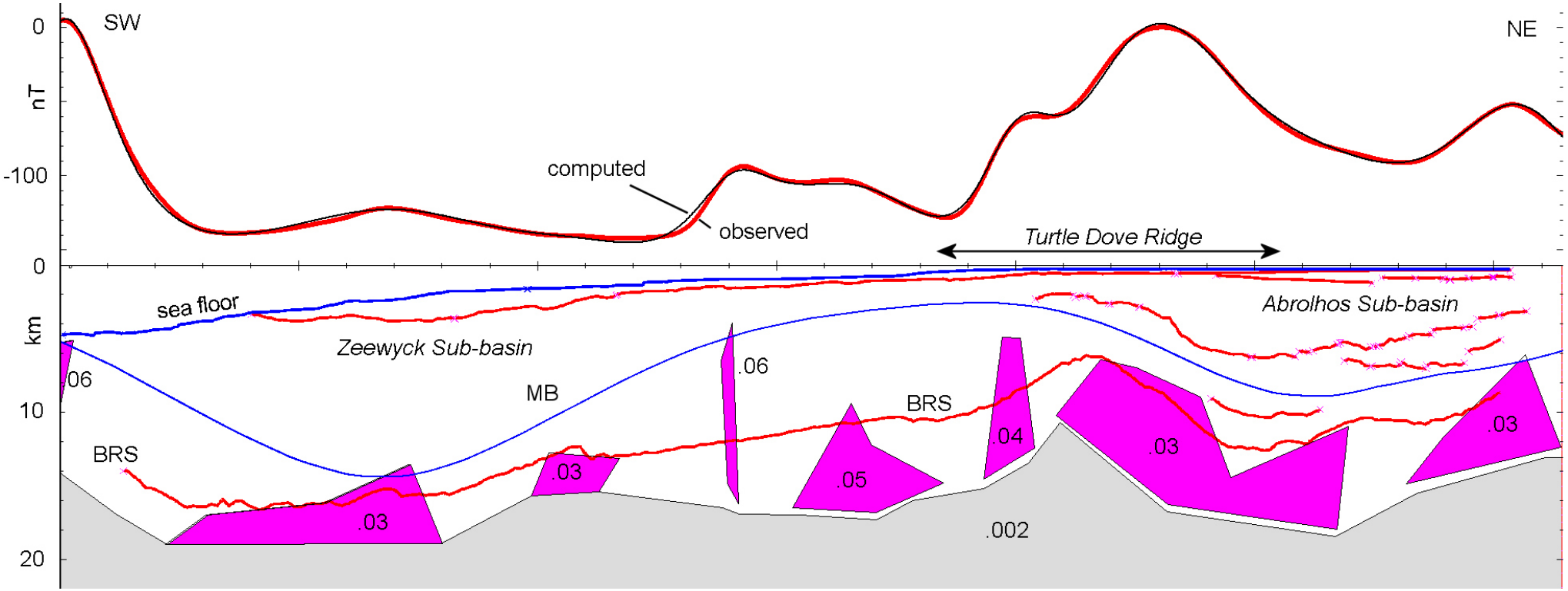

Figure 12. ***Profile C, 'deep' 3D version: magnetic susceptibility model after inversion along line GA310-29 showing deeper placement of the modelled sources with azimuths and strike extent of the four bodies at the eastern half of the line inferred from the magnetic anomaly map. The azimuth perpendicular to the line is -42.5°. From left to righ the eight bodies have azimuths: -42.5°, -42.5°, -42.5°, -20°, -20°, -35°, -42.5°, -15°, and the right-most five bodies have strike lengths 40 km.***

PROFILES D AND E: GA310-27 AND B92-3509

Profile D is along reflection seismic line GA310-27 trending SSW starting 20 km south of and in line with South Turtle Dove 1 well. The line starts at the western boundary of the Turtle Dove Ridge and crosses the northern-most part of the Vlaming Sub-basin to finish 20 km inside the Zeewyck Sub-basin.

Profile E is a shorter segment of seismic line B92-3509 intersecting GA310-27 near its northern end and trending ENE-ESW across the Turtle Dove Ridge and northernmost part of the Vlaming Sub-basin. Jones *et al*. (2011) describe and interpret reflection data along these profiles as a key transect across the southern part of acreage release area W11-18.

A significant magnetic anomaly at the southern end of the Profile D over the Zeewyck Sub-basin is modelled by a magnetic basement high topped by slabs of higher magnetic susceptibility, and two alternative models are presented. In *Figure 13* three sill-like bodies are placed along half of the profile at 5-10 km depth The shallowest is at the southern end of the profile and above the BRS, while the others below it. An alternative interpretation (*Figure 15*) is a model with just one body beneath the main anomaly below the BRS. In both interpretations, the minor field variations can be modelled by variations in depth to basement at magnetic susceptibility 0.002 SI, 1-5 km below the BRS.

The magnetic anomalies along Profile E (*Figure 15* and *Figure 16*) are modelled by deep bodies below the BRS, and a shallow interpretation is not offered. The top of magnetic basement is generally much deeper than the base of resolvable section.

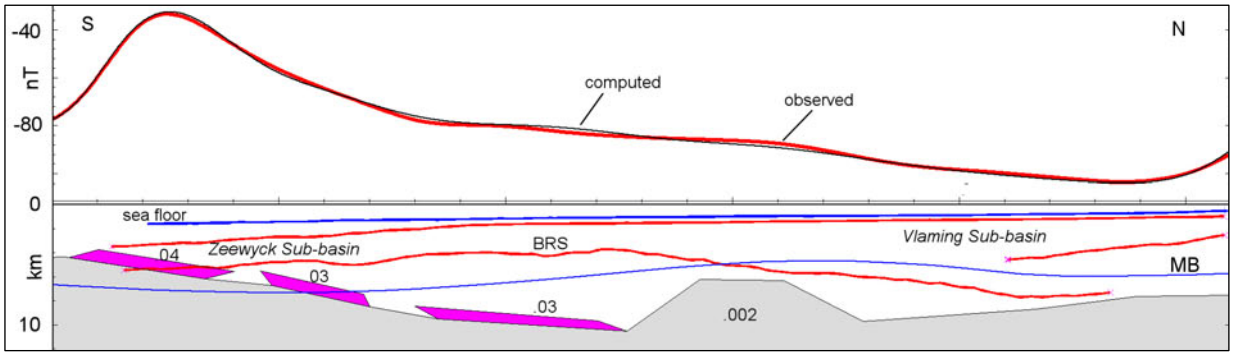

Figure 13. Profile D 'shallow' version: magnetic susceptibility model of length 52 km along seismic line GA310-27 showing magnetic (upper) and depth section (lower). V:H~0.5. 'BRS' is 'base resolvable section'.

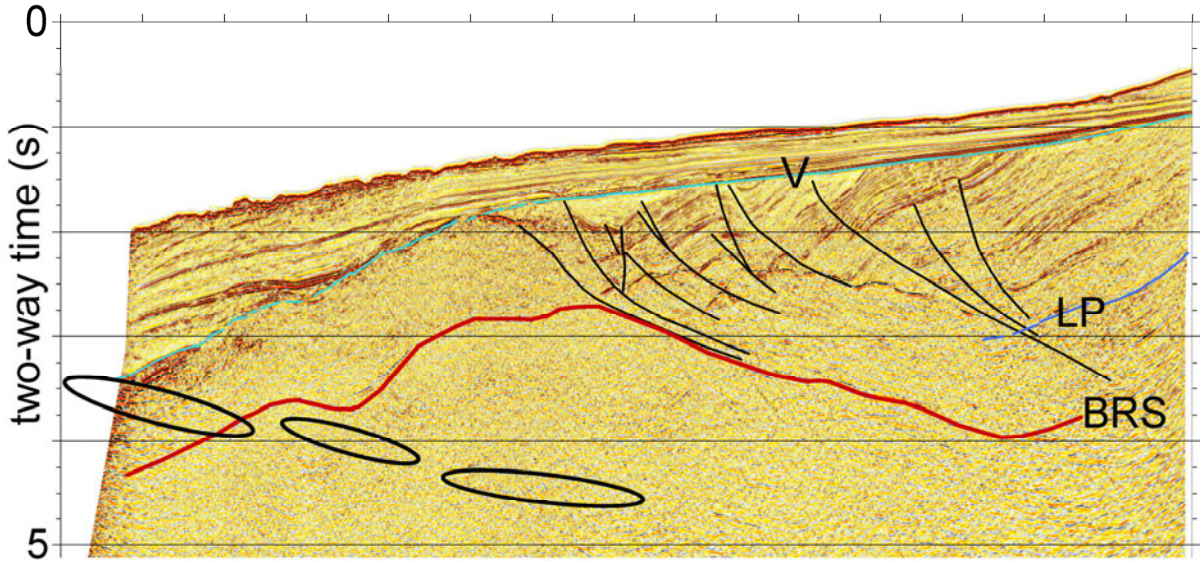

Figure 14. Profile D: reflection seismic data line GA310-27, showing 0-5s TWT and 52 km line length. 'BRS' is 'base resolvable section'.

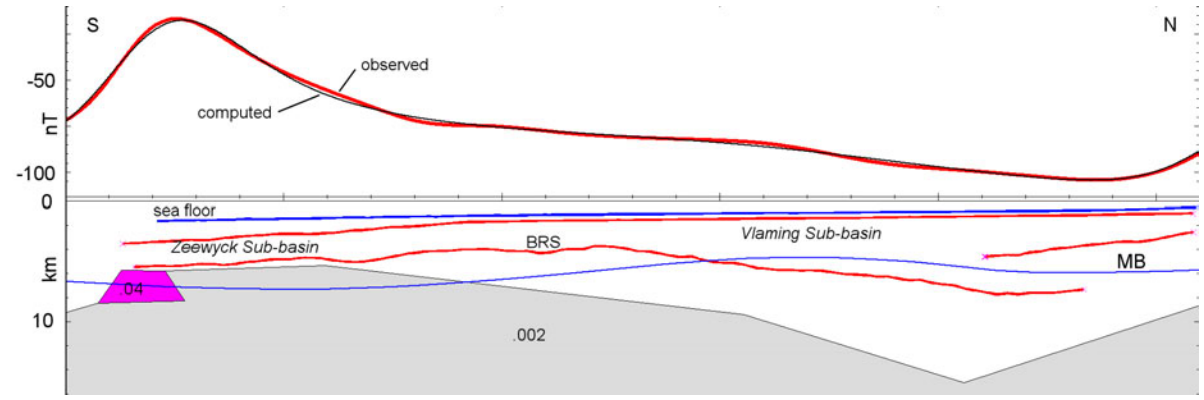

Figure 15. Profile D 'deep' version: alternative magnetic susceptibility model along seismic line GA310-27 showing magnetic (upper) and depth section (lower). V:H~0.5. 'BRS' is 'base resolvable section'. Two additional bodies are off-line (not shown).

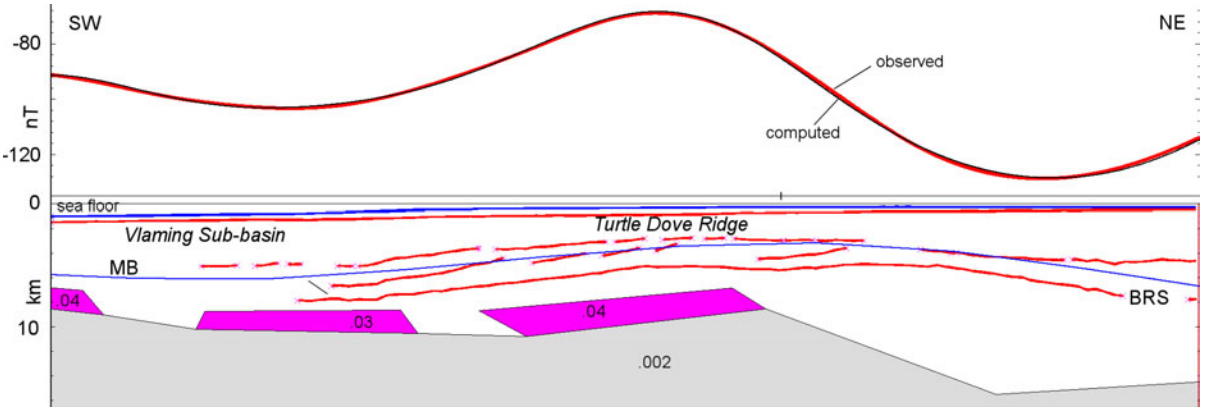

Figure 16. Profile E, 'deep' version: magnetic susceptibility model along seismic line B92-3509 of length 33 km showing magnetic anomaly (upper) depth section (lower). V:H~0.5.

3D Depth to Magnetic Basement Model

MAGNETIC SPECTRAL DEPTH TO SOURCES METHOD

A spectrally-derived depth to magnetic basement model was developed independently of the 2D magnetic models. The method used is based on the Spector and Grant (1970) method where the azimuthally averaged power spectrum of a sub-sectioned magnetic grid is analysed for straight line segments. Other authors who have used the method are Connard *et al*. (1983); Blakely (1996), Araña *et al*. (2000) and Chiozzi *et al*. (2005). While many other magnetic methods estimate depth to basement (e.g. Gunn , 1997; Nabighian *et al*., 2005), we have found that the spectral method permits geological information to be integrated into the workflow, which results in a more geologically plausible basement map.

Spector and Grant (1970) showed that the gradient of straight line segments observed in the power spectra of magnetic grids is proportional to the depth to the top of a random ensemble of magnetic sources of various geometries.

The azimuthally averaged radial power-density spectrum (S(k)) of the magnetic data within a subset window can be written as:

$$S(k) = Ae^{-2kd}(1-e^{-kT})^2 \quad (1)$$

Where k is the wavenumber, d is depth to top of source layer, T is thickness of the prism, or ensemble of magnetic sources, and A is an arbitrary constant. If T is much greater than d (T>>d), equation (1) can be written as:

$$\ln[S(k)] = \ln(A) - 2kd \quad (2)$$

So that the depth to the top of a source ensemble can be calculated by:

$$d = -\frac{\ln[S(k)]}{2k} \quad (3)$$

Random, or uncorrelated, magnetisation of the crust is assumed in the Spector and Grant (1970) method, with the power spectrum following an exponential decay. This exponential decay is in disagreement with various other authors who suggest that a power-law rate of decay is inherent in the power spectrum, a result of the fractal nature of magnetisation distribution in the crust (e.g. Pilkington and Todoeshuck, 1993). Fedi *et al*. (1997) introduced a correction factor, or β value, into the Spector and Grant method to account for this power law decay. However, the effect of this fractal correction factor has been shown to decrease with depth (e.g. Figure 7 of Fedi *et al*., 1997). As the depths of the magnetic source are large, up to 15 km, then the effect of this correction factor will be small and, as such, not considered of significance in this particular study. Also, we assume random crustal magnetisation because the fractal scaling parameter is unknown in this offshore continental margin. The results using uncorrected spectra correspond well to depth to Precambrian basement from wells and depth converted seismic.

The base magnetic grid was sub-sectioned and power spectra were subsequently calculated using Intrepid Software. Azimuthally averaged power spectra were calculated for 60 km x 60 km windows spaced with a 75% overlap throughout the study area. In this study 1049 power spectra were analysed. The window size was chosen after experimentation (see below). The amount of

overlap was chosen as a compromise between gaining a good coverage of magnetic depths and time taken for computation and analysis. Software was written to analyse the computed power spectrum; this allowed depths from the large amount of power spectra to be quickly calculated.

The depth to magnetic basement map was created by gridding calculated magnetic-spectrum depths, depths to Precambrian strata from wells (*Table 1*) and depth converted seismic interpretation from both onshore (Mory and Iasky, 1996) and offshore (C. Nicholson pers. comm.) together using the ArcMap 'Raster To Topo' gridding algorithm. A cell size of 3500 m was used in the final grid. A sediment thickness map was created by subtracting topography and bathymetry from the depth to basement grid.

DEFINING AND CONSTRAINING MAGNETIC BASEMENT

Geological basement is defined here as the top of the Precambrian interface, below which rocks are generally metasedimentary and metaigneous (e.g. Hall, in prep.). This interface has been intersected in the northern Perth Basin by a number of wells (*Table 2*) and is identified in seismic reflection data (Mory and Iasky, 1996). The Precambrian basement interface also represents the lower limit of petroleum prospectivity in the northern Perth Basin. To test whether this Precambrian interface has a magnetic signature that is identifiable using the power spectrum method, power spectra for various window sizes were calculated with the centre of windows located at sites of wells that intersect Precambrian strata and over the onshore seismic interpretation of Precambrian basement from Mory and Iasky (1996). While these wells are shallow (*Table 2*) relative to depths of sub-basins of the northern Perth Basin, the purpose of this exercise is to determine whether basement can be identified at all. This exercise also helps address the problem of determining what magnetic grid subset window size to use, as this size corresponds to the maximum observable depth to top of magnetic source. Appendix 2 shows the percentage difference between depth to Precambrian at a well site and the depth estimated from the spectral method for a range of window sizes. The results do show that a range of window sizes can adequately resolve the Precambrian interface using the spectral method, for example the 40 x 40 km window has a low percentage difference averaged over the wells sampled. However, experimentation with this window size over the deeper parts of the basin, e.g. the offshore area, showed that the 40 x 40 km (and indeed smaller window sizes) did not encompass enough magnetic sources to resolve Precambrian basement and that the 60 x 60 km window provides enough depth resolution over the shallow and deep regions of the northern Perth Basin. Thus, the outcome of this exercise shows that the Precambrian basement interface can indeed be detected by the power spectrum method, for both shallow and deep basement locations, and that a 60 x 60 km sized window is the best compromise for resolving magnetic sources at this basement interface for a variety of depths.

However, in regions without nearby well or seismic constraint one still runs the risk of choosing a spectral depth that does not correspond to source ensembles that we have defined as basement, for example intra-sedimentary volcanics. Unfortunately this is the case throughout a vast region of the offshore northern Perth Basin. The lack of constraint is due to poorly penetrating seismic reflection data in the deep and highly structured depocentres that make up the northern Perth Basin. Where seismic constraints are not available, gravity data, in particular Bouguer gravity (*Figure 2*), are used to identify where shallow or deep basement is likely to occur, allowing one to qualitatively deduce the depth of the basin. *Figure 2* shows a Bouguer gravity map with interpreted basin boundaries; the location and orientation of structural highs and depocentres can be qualitatively identified by gravity highs and lows respectively. *Figure 17* shows a power spectrum calculated in a window that spans a depocentre and structural high, which has produced two depth solutions identified by the two straight line segments in the power spectrum. The two solutions may be the result of magnetic source ensembles located on the structural high and in the depocentre that have been captured within the 60 x 60 km window. However, as the centre of the window is located in a depocentre, the deeper solution will be used for the purpose of gridding. In this way the Bouguer gravity has provided

insight into the ensemble of magnetic sources that relates to magnetic basement. While it was not always the case that multiple depth solutions were observed in a power spectrum, where they do occur the gravity data is useful in identifying which solution should be used. While gravity data can also be used to estimate depth to basement, gravity modelling of the northern Perth Basin is fraught with uncertainty due to the limited knowledge of Moho topology (e.g. Hackney *et al*., 2012.).

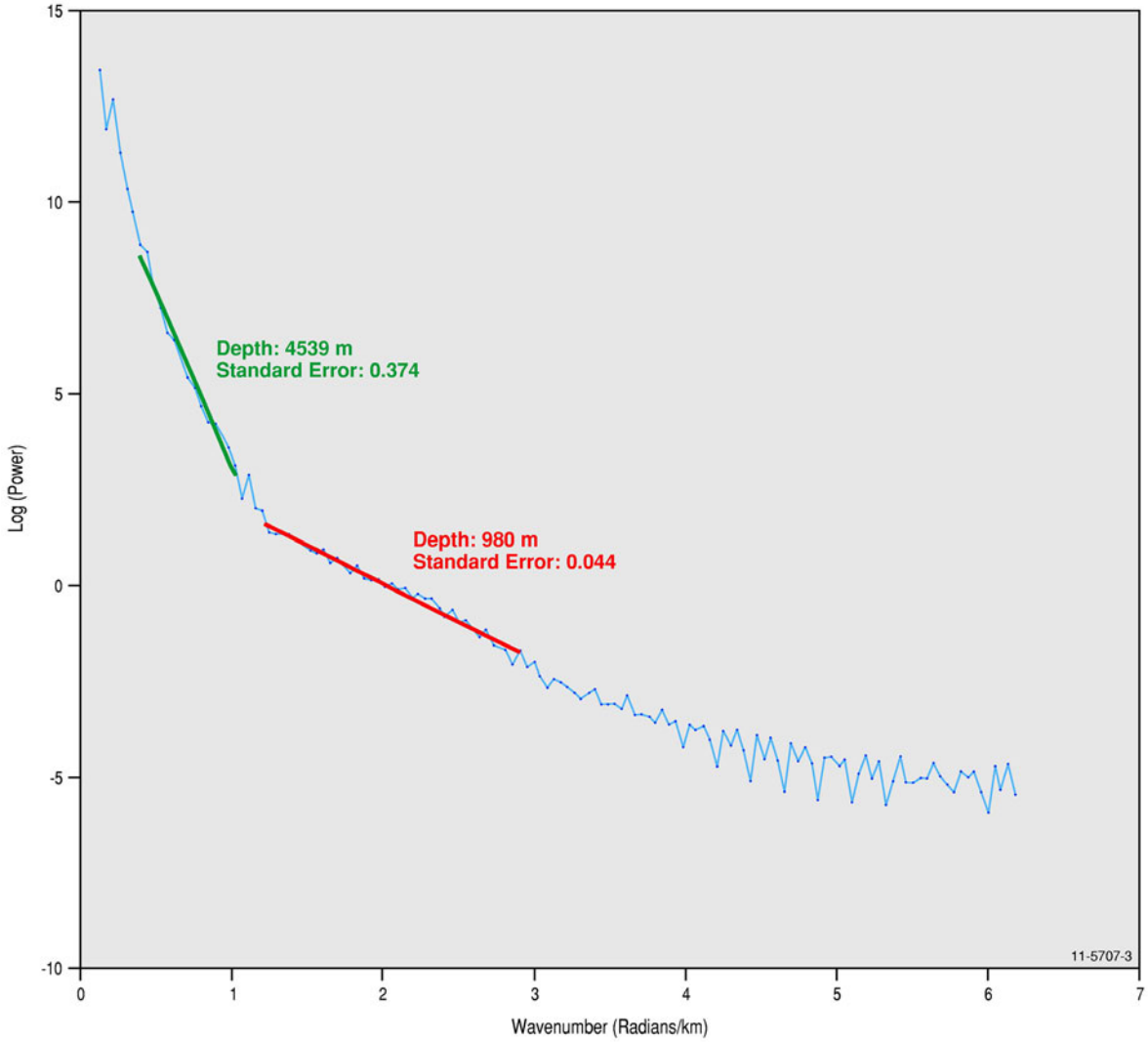

Figure 17: An example of a power spectrum containing multiple sources; one magnetic source ensemble has a top at c. 980m, the other at c. 4539m. This power spectrum was located over a Bouguer gravity low, interpreted to be a sedimentary basin, but in close proximity to a gravity high, interpreted to be a structural high. The basement was therefore interpreted to be related to the lower of the two magnetic source ensembles.

DEPTH TO BASEMENT GRID

The resulting depth to Precambrian basement grid (*Figure 18*), created by gridding magnetic power spectrum, well and seismic depths, highlights the main sub-basins and structural highs of the northern Perth Basin, as well as giving an indication of sediment thickness (*Figure 19*), where topography is subtracted from the depth to basement grid. The Abrolhos Sub-basin is clearly delineated as a c. 32 km wide, elongate, north-northwest trending depocenter, located between the Beagle Ridge to the east and the Turtle Dove Ridge to the west. A comparison of the depth to

basement map with the topography of the shallow Late Permian unconformity in the Abrolhos Sub-basin map of Jones *et al*., (2011) shows similarities in the shape of the surfaces, but with the greater depth of the basement reflecting sediment deposited during Early to Late Permian rifting.

West of the Turtle Dove Ridge the Zeewyck Sub-basin can be identified as a north-westerly-trending basin, located adjacent to oceanic crust. This sub-basin is poorly imaged on seismic reflection data, possibly due to the deep and highly structured nature of this continent-ocean transition zone. The depth to basement map shows that up to 10 km of sediment may be deposited in this sub-basin. However, a comparison with the 2.5D modelling and depth converted seismic interpretation (*Figure 6*) shows that the Zeewyck Sub-basin was not successfully modelled using the spectral method over its entire extent. Over a portion of this 2.5D model the spectral magnetic basement shallows to and intersects the Valanginian Unconformity, even though thicker sediments are inferred to be present in the region. In the depth to basement map the sediment thickness of the Houtman Sub-basin is seen to increase to the west, corresponding to deepening of basement to the west of the Houtman Fault Zone (e.g. Figure 7 of Jones *et al*., 2011). While the Abrolhos Sub-basin and Turtle Dove Ridge are relatively thin features, they are clearly represented by the basement model (e.g. *Figure 9*), most likely due to the qualitative use of the Bouguer gravity anomaly grid to constrain spectral depths.

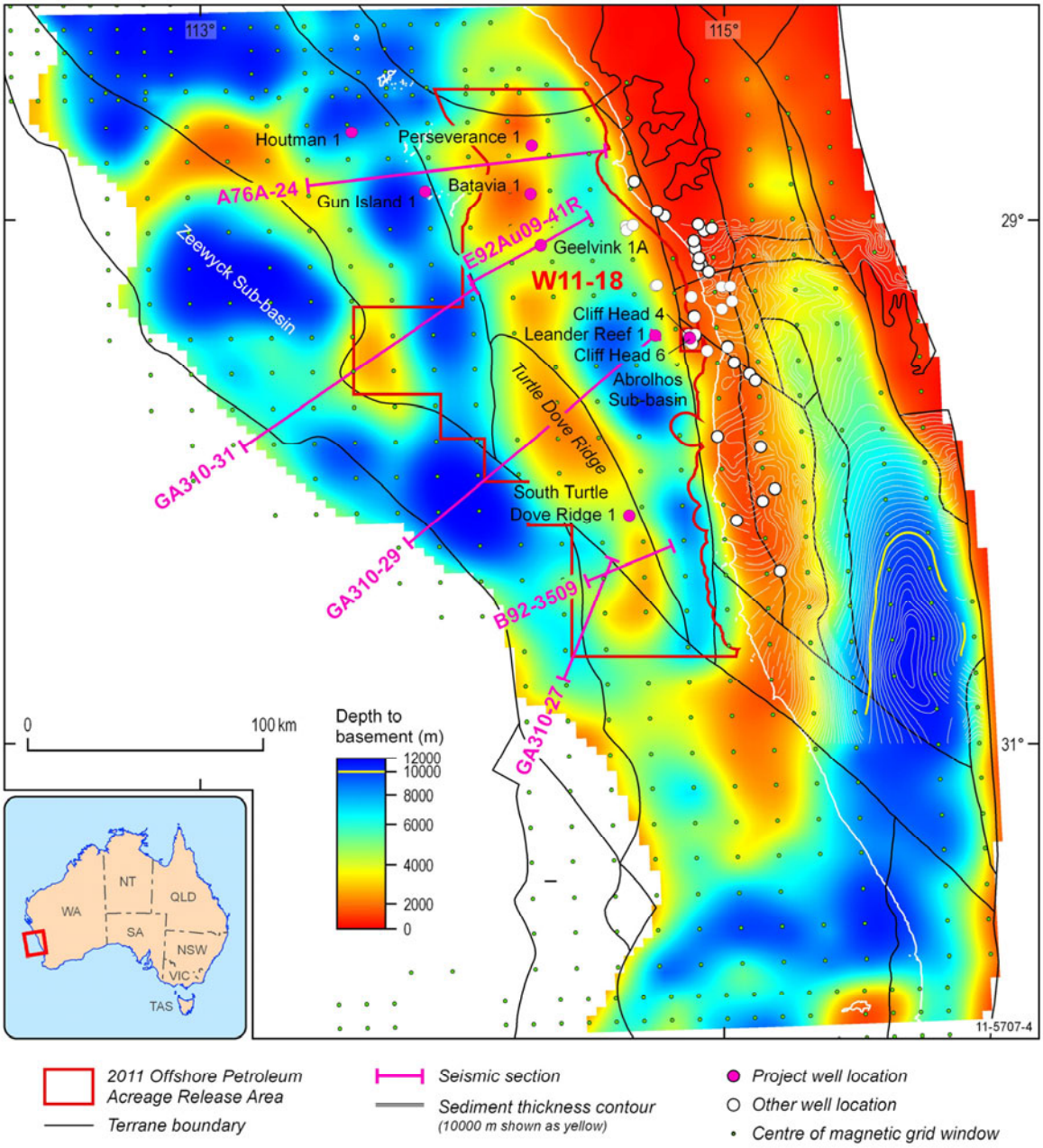

Figure 18: Depth to basement map, derived from magnetic spectral depth to source method. Blue dots are the centre locations of the 1049 60 x 60 km sub-sectioned magnetic grid windows which overlap by 75%, white circles are the location of well sites used (Table 2). White contours are the depth converted seismic interpretation of Precambrian basement from Mory and Iasky (1996), with the 10 km contour shown in yellow. Seismic lines used in the 2.5D forward magnetic models are shown as blue lines. The outline of acreage release area W11-18 is shown in red.

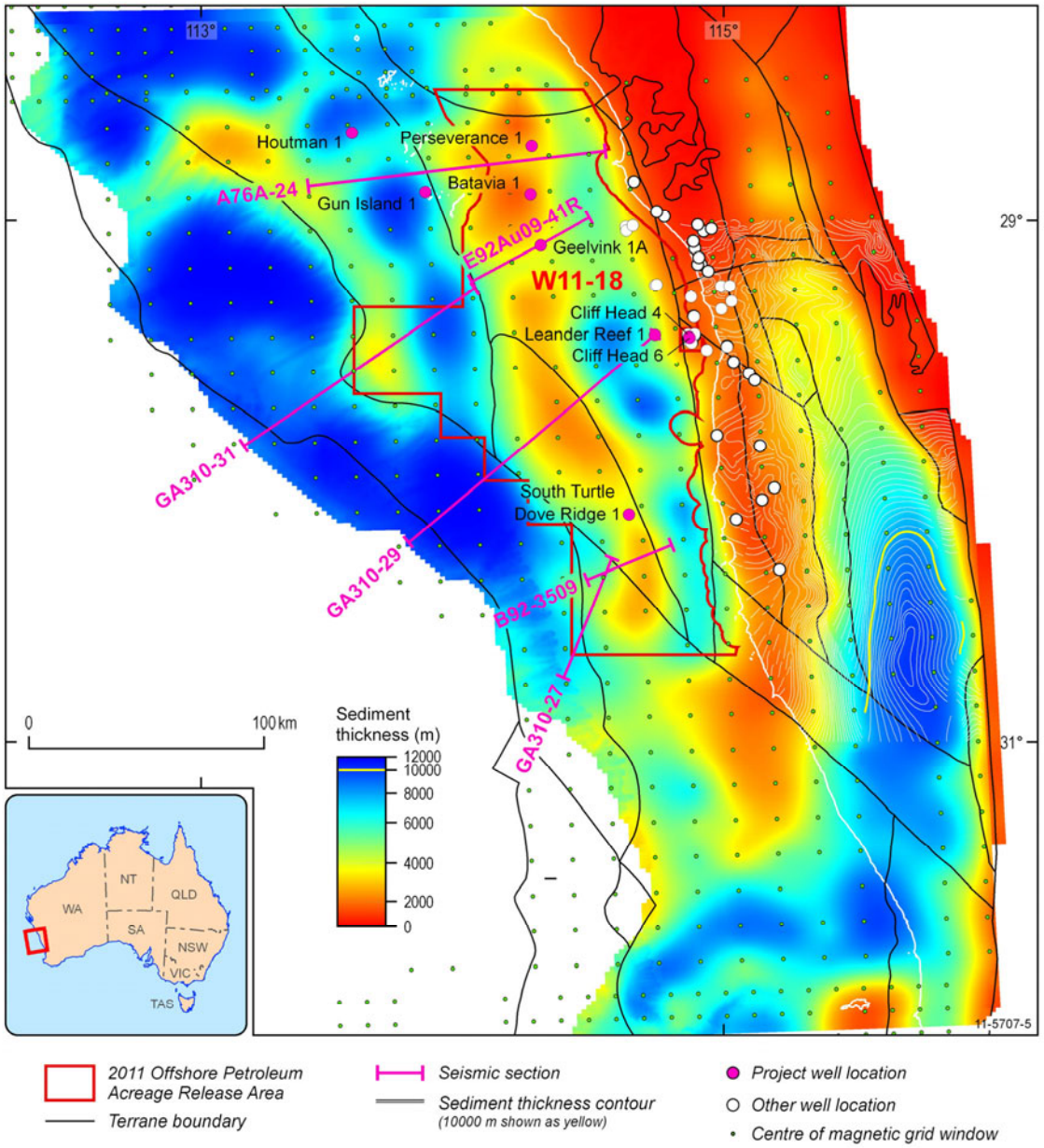

Figure 19: Sediment thickness map, derived from magnetic spectral depth to source method. Blue dots are the location of the centre of the 1049 60 x 60 km sub-sectioned magnetic grid windows which overlap by 75%, white circles are the location of well sites used (Table 2). White contours are the depth converted seismic interpretation of Precambrian basement from Mory and Iasky (1996), with the 10 km contour shown in yellow. Seismic lines used in the 2.5D forward magnetic models are shown as blue lines. The outline of acreage release area W11-18 is shown in red.

ESTIMATING ERROR IN BASEMENT GRID

Differences between depths calculated from magnetic power spectrums and the final depth grid (which is composed of gridded magnetic power spectra, well and seismic reflection depths) arise during the gridding process due the tensioned surface (i.e. the resultant grid) created through least-squares fitting not being constrained to pass through every data point. Statistics calculated on the

different input datasets, i.e. magnetic power spectrum, well and seismic depths, to assess the quality of the final grid relative to the input data are presented in *Table 7*.

Closer spaced magnetic spectrum centroids, or in other words a greater overlap of window subsets, would allow a smaller grid size to be allowable in the gridding process, rather than the 3.5 km grid cell size used in this exercise. This would most likely lead to a minimisation of differences between grid and input datasets. This was not attempted in this exercise due to the large water depths and line spacing reducing the resolution of the magnetic anomaly grid, and in turn reducing the resolution on resolvable depth from the spectral depth method.

Table 7: Statistics for the differences between the input (spectral depths, wells and seismic) datasets and gridded basement model. 'n' is the number of samples, MEAN is the average difference, MAD is the mean absolute difference, RMSE is root mean squared error, STDEV is standard deviation.

INPUT DEPTH DATA	n	MEAN (m)	MAD (m)	RMSE	STDEV
Magnetic spectrum	1049	628.	1169	2018	1918
Wells	28	-237	301	387	311
Seismic	16713	-15	342	560	559

The mean differences from *Table 7* suggest that overall the gridded basement depths are shallower than depths estimated from the un-gridded magnetic spectra and deeper than the well and seismic depths. We can also conclude that there is a greater discrepancy in the offshore region between the spectral depths and the resultant basement grid, because that is where there a few well or seismic depths and many magnetic spectrum depths.

Comparison between Magnetic Methods

The magnetic basement calculated using the spectral method is compared to that derived from the 2.5D models. This was undertaken by projecting the magnetic basement grid onto the 2.5D models, and comparing the depths of the different models.

PROFILE A: A76A-24

The magnetic basement conforms to the model to the east and west of both the shallow and deep versions of the 2.5D model, but does not fit well in the centre. The western portion of the model shows the greatest similarity between the two magnetic models of profiles shown on *Figure 4* and *Figure 5*. The presence of dipping seismic reflectors, interpreted to be sedimentary strata (*Figure 3*), observed in the centre of the profile are firm evidence that a magnetic basement is not present, and thus the spectral depth to magnetic basement in this region is erroneous. It is probable that the spectral depth solutions in this region are picking up the presence of volcanic intrusions (though the 2.5D models would identify this also), are related to other magnetic sources located offline of this profile, or are caused by shallow magnetic basement depths located toward the edges of the 60 x 60 km window being introduced into the spectra.

PROFILE B: GA310-31 + E92AU09-41R

The tops of the higher susceptibility bodies in the 'deep' and ''shallow' versions of the 2.5D magnetic model and the spectral depth to basement grid coincide over most of the north eastern

portion of this profile, where the magnetic depth grid envelopes the body tops, but diverges in the Zeewyck Sub-basin (*Figure 6* and *Figure 8*). However, *Figure 18* shows that the shallow magnetic basement in the Zeewyck Sub-basin is localised around this profile and that sediment thickness in the Zeewyck Sub-basin is greater to the north and south. The sedimentary section of the Abrolhos and Houtman Sub-basins are identified in the magnetic basement grid fairly well. However, a slight divergence between the two models is identified to the SW of the Houtman Basin, where the magnetic basement grid shallows more quickly than in the 2.5D magnetic model and seismic interpretation. This may be due to the power spectra being derived from large window sizes of the subsectioned magnetic grids and thus sampling shallow magnetic basement further to the southwest near the eastern most part of the Zeewyck Sub-basin.

PROFILE C: GA310-29

There is fairly good agreement between the magnetic basement grid and 'shallow' version of the 2.5D magnetic model on profile GA310-29 (*Figure 9*). The Abrolhos and Zeewyck Sub-basins are clearly defined, though perhaps the base of the Zeewyck is not resolved. The Turtle Dove Ridge is shown as a shallowing of the magnetic basement grid, where it envelopes the various magnetic bodies that are assumed to encompass the ridge. It is probable that thicker sediments are present over the Turtle Dove Ridge, but poor seismic imaging prevents this hypothesis being tested. The magnetic depth grid also coincides well with the 'deep' version of the 2.5D magnetic model, though it acts more as an envelope for the higher magnetic susceptibility bodies (*Figure 12*).

PROFILE D: GA310-27

The spectrally-derived magnetic basement is fairly flat along this profile, with depths in the range of 5-8 km. A slight undulation is observed above a horst-like body in the 2.5D magnetic model, which may indicate that the spectral method is detecting but not fully resolving a structure at depth (*Figure 13*). The magnetic basement grid is deeper than the 'Base Resolvable Section' seismic horizon to the south, but slightly shallower to the east. In both shallow (*Figure 13*) and deep versions (*Figure 15*) of the 2.5D magnetic model, the magnetic basement grid intersects the 2.5D modelled basement to the south. To the north of the model the shallow version of the 2.5D model more closely mimics the magnetic basement grid, while there is little similarity between grid and modelled basement in the 'deep' version of the 2.5D magnetic model.

PROFILE E: B92-3509

As with profile GA310-27, the magnetic basement grid is fairly flat along this profile (*Figure 16*). While the magnetic basement grid closely mimics the 'Base Resolvable Section' seismic horizon on line B92-3509 and the southern portion of the 2.5D model, the eastern part of the profile is not matched. However, as seismic imaging does not show a deepening of the basement to the east of the profile, one cannot conclusively say that thick sediments exist.

Overall, the magnetic basement grid and the 2.5D models match fairly well, with the spectrally derived basement grid generally being shallower than the basement from the 2.5D models and being within a few kilometres of the 'Base Resolvable Section' horizon. The magnetic basement grid seems to act as an enveloping surface over the modelled magnetic sources, which may be due to the influence of shallower magnetic sources, such as volcanoes, causing the basement grid to shallow, as seen on profile A76a-24.

Discussion and Conclusions

A depth to magnetic basement map for the northern Perth Basin has been created using the magnetic spectral technique. Bouguer gravity anomaly maps have been used to qualitatively select basement depths from power spectra showing multiple depth solutions. The depth spectral method is ideal for use on a regional scale as the depths can be quickly produced (using the software created during this study), integrated with other information (e.g. wells and seismic depths) and gridded, where it can then be used to assess sedimentary thickness and basin geometries.

A second approach based on 2.5D modelling used discrete bodies embedded in weakly magnetised basement. In this, an arbitrarily inferred magnetic basement modelled with a susceptibility of 0.002 SI near or below the limit of reflection seismic resolution (BRS in the reflection seismic figures, above) contributes a modest 5-10 nT variation compared to a total observed signal range of 50-150 nT. If, as for the Northampton Complex, basement is presumed to consist of metasediments, then a significantly higher susceptibility for basement is not expected. Indeed, susceptibility measurements of basement rocks encountered in three onshore wells indicate that a lower value cannot be used.

Limited evidence of volcanic activity was interpreted in the reflection seismic data near the level of the Valanginian break-up unconformity No such bodies were identified with confidence deeper within the sedimentary sequence. To model the amplitude and shape of the observed magnetic signal we therefore inserted, in most cases, massive bodies (0.03-0.06 SI) whose tops were near the limit of reflection seismic resolution or penetrating only the deeper sediments. These modelled 2.5D bodies, having essentially infinite strike extent, produce a higher amplitude anomaly than bodies with equivalent cross-section and limited strike extent as is likely in the geology they represent. We did not apply a correction for this effect; however it seems that some penetration of high-susceptibility bodies into the lower sediments is necessary to model the observed magnetic anomaly.

Although there is little reflection seismic evidence for the modelled magnetised bodies, in some cases they may be associated with interpreted faults. An example is noted in Profile B (*Figure 8*) where the modelled body dipping to the southwest with susceptibility 0.3 SI is close to and dipping parallel to a major boundary identified as the Houtman Fault Zone in the reflection seismic data (*Figure 7*). Where the modelled bodies penetrate the sediments, they are mostly below or within the Permian section, except for the western ends of lines where sediments are thin over oceanic crust. In the latter cases, a higher susceptibility ~0.06 SI was used, the rocks presumably becoming more mafic towards oceanic crust.

We postulate that the bodies modelled are igneous magnetised plutons or dense assemblages of mafic dykes and sills penetrating basement that are not resolved as individual bodies. The tectonic setting of their emplacement, either during Gondwanan breakup in the Valanginian or as a component of older basement terranes, remains an open question. A related question impacting the plausibility of deep magnetised bodies is the Curie magnetisation limit in this region. On the Indian margin, a Curie isotherm map, described by Rajaram *et al*. (2009), developed using the spectral method, shows a minimum Curie depth of 22 km. The results presented here suggest that the magnetised bodes are well above that depth.

On the northern-most seismic lines modelled, A76A-24, and GA310-31 extended by E92AU09-41R (profiles A and B, respectively), the Batavia Ridge magnetic anomaly is modelled by massive bodies whose tops are 5-10 km below sea floor. On these and other profiles to the south, the dyke-like bodies were placed in our models rarely shallower than 5 km below the sea floor.

Magnetic forward modelling of 2.5D transects suggests the presence of a zone of relatively higher magnetic susceptibility material with a thin, vertical to sub-vertical geometry within or below the South Turtle Dove ridge structural high.

Figure 6 and *Figure 9* for the modelled seismic lines GA310-31 extended by E92AU09-41R, and GA310-29 (profiles B and C) respectively show the intersection with the surface of depth to magnetic sources by the spectral method model (labelled 'MB'). Generally the spectrally derived magnetic basement is shallower than the tops of modelled 2.5D magnetic bodies, and tends to envelope them. What could be the reason for the spectral depths being shallower than the modelled bodies? The placement of the 2.5D magnetised bodies was influenced by an initial assumption that their tops may be located near the base of resolvable section ('BRS' in the figures). The discrepancy between the magnetic basement model and the 2.5D models may be because the stacking velocities used to depth convert the 'base resolvable section' horizon were too high relative to the actual P-wave velocity in the crust. We did not investigate a suite of models in which the observed field was modelled by broader bodies of lower magnetic susceptibility such as sills and volcanic flows placed within the sedimentary sequence. There is limited evidence of these igneous features in the reflection seismic data. Evidence for volcanic flows was interpreted on GA310-31 extending laterally just 1500 m (N. Rollet, *pers. comm.*). Some bright reflectors, interpreted to be due to volcanic rock, are observed on GA310-29 at the Valanginian break-up unconformity. However, because of the limited extent of these interpreted volcanic bodies, they were not included in the forward modelling.

An increase in the spatial resolution of the depth-to-basement map could be gained by using greater overlap between consecutive sub-sectioned windows. However, this would come at a cost of an increase in the time required to compute and analyse the computed power spectra.

Whilst constructing the depth to basement map using a priori knowledge of the geology and qualitative and quantitative sediment thickness brings this method out of the realm of pure geophysical modelling into that of integrated geological and geophysical interpretation, it is our opinion that this approach is needed to gain a meaningful map of basement depth. Other automated methods for estimating depth to magnetic basement (e.g. those discussed in Gunn, 1997; Nabighian *et al*., 2005) provide good results for simple magnetic anomalies and related geology. However, over a large region such as the northern Perth Basin, and with such varied basement character, an integrated and automated approach is more practical.

Comparisons between the 2.5D magnetic models and the spectral magnetic depth to basement method show that the spectral method provides a first order approximation to basement depth and topology. The spectral method did not give results that exactly matched those from the forward models, but provided a good approximation to depths and shapes of the depocenters of the northern Perth Basin. Some successes included modelling the depths to and topology of the Abrolhos and Houtman sub-basins. However, the Zeewyck Sub-basin was not modelled particularly well in the vicinity of Profile B (GA310-31), though deeper sediment which is more representative of the sub-basin is found to the north and south of this profile. This discrepancy may be due to the proximity of this sub-basin to the western limit of the magnetic dataset and continent-ocean boundary, and the deep water in which the basin is situated.

Acknowledgements

The authors thank Ron Hackney and Tony Meixner for reviewing the document, Lisa Hall and Andrew Jones for criticism and commentary, Jamie Lankford for retrieving core samples and providing access to the laboratories for measurement of magnetic susceptibilities, Chris Nicholson and George Bernardel for discussion of seismic interpretation and support in measurement of susceptibilities, David Arnold and Theo Chiotis for drafting some of the figures and Daniel Rawson for graphic design. This paper is published with the permission of the CEO, Geoscience Australia.

References

Araña, V., Camachob, A.G., Garciaa, A ., Montesinosb, F.G , Blancoa, I., Vieirab, R. and Felpetoa, A. 2000. 'Internal structure of Tenerife (Canary Islands) based on gravity, aeromagnetic and volcanological data'. *Journal of Volcanology and Geothermal Research*, 103(1-4), 43-64.

Blakely, R.J. 1996. Potential Theory in Gravity and Magnetic Applications. Cambridge University Press: Cambridge.

Borissova, I., Bradshaw, B.E., Nicholson, C.J, Struckmeyer, H.I.M., and Payne, D. 2010. New exploration opportunities on the southwest Australian marin – deep water frontier Mentelle Basin. *The APPEA Journal*, 50.

Chiozzi, P., Matsushima, J., Okubo, Y., Pasquale, V. and Verdoya., M. 2005. 'Curie-point depth from spectral analysis of magnetic data in central-southern Europe'. *Physics of the Earth and Planetary Interiors*, 152, 267-276.

Connard, G., Couch, R. and Gemperle, M. 1983. 'Analysis of aeromagnetic measurements from the Cascade Range in central Oregon'. *Geophysics*, 48, 376-390.

Carmichael, R.S. 1989. 'Magnetic properties of minerals and rocks – Section IV' *in* Carmichael, R.S. (ed), *Practical handbook of physical properties of rocks and minerals*, 1989. CRC Press: U.S.A.

Clark, D.A. 1999. 'Magnetic petrology of igneous intrusions: implications for exploration and magnetic interpretation'. *Exploration Geophysics*, 30, 5-26.

Dadd, K. and Kellerson, L. 2011. A petrographic and geochemical investigation of volcanic rocks dredged from the Western Australian margin. Department of Earth and Planetary Sciences Macquarie University. (unpub.), Geoscience Australia: Canberra.

Daniell, J., Jorgensen, D., Anderson, T., Borissova, I., Burq, S., Heap, A., Hughes, M., Mantle, D., Nelson, G., Nichol, S., Nicholson, C., Payne, D., Przeslawski, R., Radke, L., Siwabessy, J., Smith, C. and Shipboard Party. 2009. Frontier basins of the west Australian continental margin: post survey report of marine reconnaissance and geological sampling survey GA2476, Record 2009/38. Geoscience Australia: Canberra.

Dentith, M.C., Long, A., Scott, J., Harris, L.B. and Wilde, S.A., 1994. 'The influence of basement on faulting within the Perth basin, Western Australia', in: Purcell, P.G. and Purcell, R.R. (eds), *The sedimentary basins of Western Australia. Proceedings of the Western Australian basins Symposium*, 791-799.

Enterprise Oil, 1993a. *Final report Plum seismic survey, WA-230-P, 19 August – 10 October, 1992*. (unpub.)

Enterprise Oil, 1993b. *Final report aeromagnetic survey, WA-230-P, Western Australia, November 12, 1992 to December 9, 1992*. (unpub.)

Fedi, M., Quarta, T. and Angelo, D. 1997. 'Inherent power-law behaviour of magnetic field power spectra from a Spector and Grant ensemble'. *Geophysics*, 62(4), 1143.

Foster, C., Goleby, B., Borissova, I. and Heap, A. 2009. 'Southwest Margins surveys completed'. *AusGeo News*, 94. Available at: www.ga.gov.au/ausgeonews/ausgeonews200906/surveys.jsp

Gorter, J. and Deighton, I., 2002. 'Effects of igneous activity in the offshore northern Perth Basin – evidence from petroleum exploration wells, 2D seismic and magnetic surveys', in, Keep, M. and Moss, S.J. (eds) The sedimentary basins of Western Australia: a frontier petroleum province on the doorstep? *The APPEA Journal*, 44(1), 13-57.

Gregorova, D., Hrouda, F., Kohut, M., 2003. 'Magnetic susceptibility and geochemistry of Variscan West Carpathian granites: implications for tectonic setting'. *Physics and Chemistry of the Earth*, Parts A/B/C, 28(16-19), 729-734, DOI: 10.1016/S1474-7065(03)00125-6.

Gunn, P.J. 1997. 'Quantitative methods for interpreting aeromagnetic data: a subjective review'. *AGSO Journal of Australian Geology and Geophysic*s, 17(2), 105-113.

Gunn, P., Palmer, R. and Brett, J. 2004. Interpretation of the East Abrolhos aeromegnetic survey in WA-325-P, Abrolhos Sub-basin, North Perth basin, Western Australia. *Intrepid Geophysics: Melbourne*.

Hackney R & Morse M, 2011. Levelled ship-track magnetic and gravity data for parts of Australia's continental margins. *Abstracts, XXV General Assembly, International Union of Geodesy and Geophysics, 28 June – 7 July,* Melbourne.

Hackney R, Hall L & Köther N, 2012. Potential-field data for structural interpretation in the northern Perth Basin, Australia. *Extended Abstracts, 22nd International Conference and Exhibition, Australian Society of Exploration Geophysicists, 22–29 February,* Brisbane, 4pp.

Hall, L., in prep. *Basement Terranes, Structure and Composition of Australia's Southwest Margin. Record*. Geoscience Australia: Canberra.

Heap, A.D. and Harris, P.T. 2008. 'Geomorphology of the Australian margin and adjacent seafloor'. *Australian Journal of Earth Sciences*, 55, 555-585.

Iasky, R.P., D'Ercole, C., Ghori, K.A.R., Mory, A.J. and Lockwood, A.M. 2003. 'Structure and petroleum prospectivity of the Gascoyne Platform, Western Australia'. Western Australia Geological Survey, Report 87, 56p.

Johnston, S.W. and Goncharov, A. 2012. Velocity analysis and depth conversion in the offshore northern Perth Basin, Australia. Record 2012/33. Geoscience Australia: Canberra.

Jones, D. 1983. *Interpretation of gravity and magnetic data in permit WA-165P for Ocelot International Pty Ltd*, *ECL Australia Pty Ltd.* (unpub.).

Jones, A.T., Kennard, J.M., Nicholson, C.J., Bernardel, G., Mantle, D., Grosjean, E., Boreham, C.J., Jorgensen, D.C. and Robertson, D. 2011. 'New exploration opportunities in the offshore northern Perth Basin'. *The APPEA Journal*, 51, 45-78.

Jorgensen, D.C., Jones, A.T., Kennard, J.M., Mantle, D., Robertson, D., Nelson, G., Lech, M., Grosjean, E., and Boreham, C.J. 2011. Offshore northern Perth Basin well folio. *Record 2011/09.* Geoscience Australia: Canberra.

Lindsley, D.H., Andersen, G.E. and Balsley, J.R. 1966. Magnetic properties of rocks and minerals, in, Clark, S.P. (ed) *Handbook of physical constants.Memoir 97.* Geological Society of America: New York..

Milligan PR, Franklin R, Minty BRS, Richardson LM & Percival PJ. 2010. Magnetic Anomaly Map of Australia (Fifth Edition), 1:15 000 000 scale. Geoscience Australia, Canberra.

Mory, A.J. and Iasky, R.P. 1996. Stratigraphy and structure of the onshore northern Perth Basin, Western Australia. *Report 46.* Western Australia Geological Survey: Perth.

Nabighian, M. N., Grauch, V. J. S., Hansen, R. O., LaFehr, T. R, Li, Y., Peirce, J. W., Phillips, J. D. and Ruder, M. E. 2005. 'The historical development of the magnetic method in exploration'. *Geophysics*, 70(6), 33-61.

Nicholson, C.J., Borissova, I., Krassay, A.A., Boreham, C.J., MOnteil, E., Neumann, V., di Primio, R., and Bradshaw, B.E. 2008. New exploration opportunities in the southern Vlaming Sub-basin. *APPEA Journal* 48, 371-379.

Petkovic P, Fitzgerald D, Brett J, Morse M & Buchanan C. 2001. Potential Field and Bathymetry Grids of Australia's Margins. ASEG Extended Abstracts 2001**:**1,, doi:10.1071/ASEG2001ab109.

Pilkington, M. and Todoeshuck, J.P. 1993. 'Fractal magnetization of continental crust'. *Geophysical Research Letters*, 20(7), 627-630.

Rajaram, M., Anand, S.P., Hemant, K. and Purucker, M.E. 2009. 'Curie isotherm map of Indian subcontinent from satellite and aeromagnetic data', *Earth and Planetary Science Letters*, 281, 147-158, doi:10.1016/j.epsl.2009.02.013.

Roc Oil Pty Ltd, 2003. *North Perth Basin WA-325-P & WA-327-P Rita & Cheryl MSS seismic interpretation report*. Geoscience Australia: Canberra.

Schmidt, P.W. 2010. *Rock property measurements on dredge samples acquired on Geoscience Australia survey GA-2476 (RV Sonne) from the Wallaby Plateau and surrounds.* (unpub.) Geoscience Australia: Canberra.

Spector, A. and Grant, F.S. 1970. 'Statistical models for interpreting aeromagnetic data'. *Geophysics*, 35(2), 293-302.

Symonds, P.A., Planke, S., Frey, Ø. and Skogseid, J. 1998. 'Volcanic evolution of the western Australia continental margin and its implications for basin development', in: *The sedimentary basins of Western Australia 2: Proceedings of Petroleum Exploration Society of Australia Symposium, Perth, 1998*, 33-54.

Telford, W.M., Geldart, L.P., Sheriff, R.E. and Keys, D.A. 1976. *Applied Geophysics*. Cambridge UP: UK.

Appendix 1 – Magnetic susceptibility measurements

All measurements were taken using a KT5 magnetic susceptibility meter, and are reported as SI x10^{-3} units. Sequences and rock types are taken from Jorgensen *et al*., (2011).

Batavia 1								
DEPTH (m)	**1**	**2**	**3**	**4**	**5**	**6**	**AVERAGE (SI)**	**SEQUENCE**	**ROCK TYPE**
2794	0.02	0.03	0.03				0.026666667	Irwin River	Sandy carbonaceous siltstone and coal measures
2794.5	0.04	0.04	0.04				0.04		
2795	0.04	0.04	0.04				0.04		
2795.5	0.04	0.02	0.02	0.03			0.0275		
2796	0.03	0.03	0.03	0.03			0.03		
2796.5	0.02	0.03	0.04	0.03			0.03		
2797	0.04	0.03	0.03	0.02			0.03		
2797.5	0.03	0.03	0.03				0.03		
2798	0.03	0.02	0.03	0.04			0.03		
2798.5	0.04	0.04	0.04				0.04		
2799	0.04	0.03	0.02	0.02			0.0275		
2799.5	0.04	0.04	0.03	0.04			0.0375		
2800	0.07	0.03	0.03	0.04	0.03	0.04	0.04		
2800.5	0.03	0.02	0.03	0.03			0.0275		
2801	0.05	0.05	0.04	0.04			0.045		
2801.5	0.02	0.02	0.02				0.02		

BMR 10/10A								
DEPTH (m)	**1**	**2**	**3**	**4**	**5**	**6**	**AVERAGE (SI)**	**SEQUENCE**	**ROCK TYPE**
4691	0.15	0.12	0.12	0.14			0.1325	Basement	Metamorphic Basement
4803	0.13	0.14	0.1	0.13			0.125		
4806	0.09	0.11	0.1				0.1		
4809	0.1	0.08	0.13	0.09			0.1		

4813	0.11	0.1	0.08	0.09		0.095		
4852	0.59	0.59	0.59	0.59		0.59		

Cliff Head 4								
DEPTH (m)	**1**	**2**	**3**	**4**	**5**	**6**	**AVERAGE (SI)**	**SEQUENCE**	**ROCK TYPE**
1414	0.03	0.05	0.08	0.09			0.0625	Irwin River	Sandy carbonaceous siltstone and coal measures
1414.5	0.14	0.14	0.14	0.14			0.14		
1415	0.29	0.27	0.28				0.28		
1415.5	0.39	0.4	0.37	0.36			0.38		
1416	0.17	0.16	0.16	0.16			0.1625		
1416.5	0.12	0.14	0.14	0.13			0.1325		
1417	0.15	0.16	0.13	0.16	0.14		0.148		
1417.5	0.14	0.14	0.14				0.14		
1418	0.11	0.1	0.11	0.13			0.1125		
1418.5	0.14	0.13	0.15	0.14			0.14		
1419	0.17	0.18	0.19	0.18			0.18		
1419.5	0.13	0.13	0.14				0.133		
1420	0.12	0.12	0.11	0.1			0.1125		
1420.5	0.09	0.12	0.12	0.12			0.1125		
1421	0.16	0.16	0.14	0.15			0.1525		
1421.5	0.07	0.08	0.06	0.08			0.0725		
1422	0.11	0.1	0.1	0.09			0.1		
1422.5	0.11	0.09	0.09	0.1			0.0975		
1423	0.18	0.17	0.17	0.18			0.175		
1423.5	0.19	0.18	0.2	0.2			0.1925		
1424	0.15	0.15	0.18	0.16			0.16		
1424.5	0.19	0.19	0.2	0.19			0.1925		
1425	0.2	0.21	0.18	0.2			0.1975		
1425.5	0.12	0.11	0.12	0.12			0.1175		
1426	0.04	0.04	0.04				0.04		
1426.5	0.04	0.03	0.04				0.0367		

1427	0.03	0.03	0.03	0.02		0.0275
1427.5	0.04	0.04	0.04			0.04
1428	0.04	0.04	0.04			0.04
1428.5	0.05	0.04	0.04			0.0433
1429	0.09	0.09	0.09			0.09
1429.5	0.06	0.06	0.07	0.07		0.065
1430	0.05	0.07	0.07	0.06		0.0625
1430.5	0.09	0.08	0.08	0.08		0.0825
1431	0.05	0.07	0.07	0.05		0.06
1431.5	0.05	0.06	0.05			0.053
1432	0.03	0.02	0.03			0.0267
1432.5	0.04	0.04	0.05			0.0433
1433	0.06	0.07	0.07			0.0667
1433.5	0.03	0.05	0.04			0.04
1434	0.04	0.03	0.03	0.03		0.0325
1434.5	0.04	0.03	0.03	0.05		0.0375
1435	0.08	0.07	0.08	0.07		0.075
1435.5	0.05	0.05	0.05			0.05
1436	0.07	0.08	0.07	0.07	0.06	0.07
1436.5	0.07	0.06	0.06			0.0634
1437	0.1	0.11	0.1	0.1		0.1025
1437.5	0.1	0.1	0.09	0.09		0.095
1438	0.16	0.17	0.16	0.16		0.1625
1438.5	0.07	0.08	0.07	0.07		0.0725
1439	0.12	0.12	0.12			0.12

Cliff Head 6								
DEPTH (m)	**1**	**2**	**3**	**4**	**5**	**6**	**AVERAGE (SI)**	**SEQUENCE**	**ROCK TYPE**
1368	0.09	0.12	0.11	0.1	0.11		0.106	Kockatea	Shale, claystone and siltstone with minor sandstone and limestone
1368.5	0.17	0.17	0.18	0.17	0.16	0.17	0.17		
1369	0.14	0.12	0.12	0.11	0.12	0.13	0.1233		

1369.5	0.19	0.18	0.18				0.1833		
1370	0.19	0.21	0.19	0.1	0.09	0.08	0.1433		
1370.5	0.13	0.12	0.12				0.1233		
1371	0.13	0.13	0.13				0.13		
1371.5	0.09	0.08	0.09				0.0867		
1372	0.17	0.17	0.16				0.1667		
1372.5	0.02	0.02	0.03				0.0233		
1373	0.09	0.06	0.05	0.05			0.0625		
1373.5	0.05	0.05	0.04				0.04667		
1374	0.06	0.07	0.06				0.06333		
1374.5	0.06	0.05	0.04	0.05			0.05		
1375	0.06	0.05	0.05	0.05			0.0525	Irwin River	Sandy carbonaceous siltstone and coal measures
1375.5	0.08	0.05	0.06	0.06			0.0625		
1376	0.06	0.06	0.06				0.06		
1376.5	0.05	0.05	0.05				0.05		
1377	0.07	0.06	0.05	0.06			0.06		
1377.5	0.06	0.05	0.05				0.0533		
1378	0.12	0.12	0.12	0.11			0.1175		
1378.5	0.07	0.07	0.08				0.0733		
1379	0.07	0.07	0.06	0.06			0.065		
1379.5	0.06	0.05	0.05	0.05			0.0525		
1380	0.06	0.06	0.06				0.06		
1380.5	0.09	0.08	0.08	0.08			0.0825		
1381	0.04	0.04	0.04				0.04		
1381.5	0.02	0.01	0	0.01			0.01		
1382	0.04	0.04	0.03				0.036666667		
1382.5	0.06	0.05	0.05				0.053333333		
1383	0.04	0.04	0.03				0.036666667		
1383.5	0.05	0.04	0.06	0.05			0.05		
1384	0.06	0.06	0.06				0.06		

1384.5	0.04	0.04	0.04			0.04		
1385	0.07	0.07	0.05	0.04	0.05	0.056		
1385.5	0.05	0.05	0.06			0.053333333		
1386	0.03	0.04	0.04	0.05		0.04		
1386.5	0.03	0.04	0.03	0.04		0.035		
1387	0.04	0.04	0.03			0.036666667		
1387.5		0.04	0.03	0.04		0.036666667		
1388	0.01	0	0			0.003333333		
1388.5	0.03	0.04	0.04			0.036666667		
1389	0.02	0.03	0.03			0.026666667		
1389.5	0.04	0.02	0.03	0.03		0.03		
1390	0.02	0.04	0.02	0.03		0.0275		
1390.5	0.04	0.04	0.05			0.043333333		
1391	0.05	0.04	0.05	0.04		0.045		
1391.5	0.04	0.02	0.03	0.01		0.025		
1392	0.03	0.02	0.03			0.026666667		
1393	0.2	0.19	0.19			0.193333333	Irwin River	Sandy carbonaceous siltstone and coal measures
1393.5	0.19	0.16	0.15	0.17		0.1675		
1394	0.11	0.12	0.13	0.11		0.1175		
1394.5	0.12	0.11	0.1	0.1	0.09	0.104		
1395	0.12	0.12	0.13			0.123333333		
1395.5	0.14	0.12	0.13	0.12		0.1275		
1396	0.11	0.11	0.11			0.11		
1396.5	0.16	0.12	0.11	0.11	0.12	0.124		
1397	0.12	0.15	0.15	0.14		0.14		
1397.5	0.07	0.08	0.08			0.076666667		
1398	0.04	0.06	0.05	0.04		0.0475		
1398.5	0.06	0.06	0.05			0.056666667		
1399	0.08	0.07	0.07			0.073333333		
1399.5	0.08	0.07	0.07			0.073333333		

1400	0.04	0.04	0.04			0.04
1400.5	0.13	0.12	0.11	0.11		0.1175
1401	0.1	0.1	0.1			0.1
1401.5	0.06	0.06	0.04			0.053333333
1402	0.04	0.02	0.03	0.02		0.0275
1402.5	0.03	0.05	0.05	0.04		0.0425
1403	0.03	0.03	0.03			0.03
1403.5	0.06	0.05	0.05			0.053333333
1404	0.04	0.04	0.03	0.04		0.0375
1404.5	0.03	0.03	0.02	0.03		0.0275
1405	0.02	0.04	0.04	0.04		0.035
1405.5	0.04	0.04	0.04	0.04		0.04
1406	0.04	0.05	0.04	0.04	0.04	0.042
1406.5	0.04	0.04	0.04	0.04	0.07	0.046
1407	0.03	0.02	0.02	0.03		0.025
1407.5	0.06	0.04	0.04	0.04	0.03	0.042
1408	0.04	0.02	0.02	0.04	0.04	0.032
1408.5	0.04	0.03	0.03	0.03		0.0325
1409	0.04	0.03	0.04			0.036666667
1409.5	0.04	0.05	0.03	0.04		0.04
1410	0.03	0.03	0.03			0.03
1410.5	0.05	0.03	0.04	0.03	0.05	0.04
1411	0.02	0.02	0.03			0.023333333
1411.5	0.03	0.02	0.04			0.03
1412	0.03	0.04	0.03			0.033333333
1412.5	0.04	0.03	0.04			0.036666667
1413	0.01	0.01	0.04	0.03	0.03	0.024
1413.5	0.05	0.05	0.06			0.053333333
1414	0.03	0.03	0.03			0.03
1414.5	0.04	0.03	0.04			0.036666667
1415	0.03	0.05	0.03	0.04		0.0375
1415.5	0.04	0.04	0.04			0.04

1416.5	0.03	0.03	0.03			0.03	Irwin River	Sandy carbonaceous siltstone and coal measures
1417	0.01	0.02	0.02	0.02		0.0175		
1417.5	0.04	0.05	0.05	0.04		0.045		
1418	0.04	0.04	0.04			0.04		
1418.5	0.04	0.03	0.03	0.03		0.0325		
1419	0.04	0.04	0.03			0.036666667		
1419.5	0.04	0.05	0.03			0.04		
1420	0.02	0.03	0.03			0.026666667		
1420.5	0.04	0.04	0.05	0.05		0.045		
1421	0.03	0.02	0.02	0.03		0.025		
1421.5	0.03	0.03	0.03			0.03		
1422	0.02	0.02	0.03			0.023333333		
1422.5	0.03	0.04	0.05	0.03		0.0375		
1423	0.04	0.04	0.04			0.04		
1423.5	0.3	0.03	0.02	0.02		0.0925		
1424	0.02	0.03	0.02	0.03		0.025		
1424.5	0.01	0.03	0.03	0.03		0.025		
1425	0.03	0.03	0.04			0.033333333		
1425.5	0.05	0.03	0.03	0.03		0.035		
1426	0.05	0.03	0.04	0.06		0.045		
1426.5	0.04	0.04	0.04			0.04		
1427	0.04	0.05	0.04	0.04		0.0425		
1427.5	0.05	0.05	0.05	0.06		0.0525		
1428	0.05	0.04	0.05	0.05		0.0475		

Edel 1								
DEPTH (m)	**1**	**2**	**3**	**4**	**5**	**6**	**AVERAGE (SI)**	**SEQUENCE**	**ROCK TYPE**
987.552	0.07	0.04	0.07	0.04	0.03	0.04	0.048333333	Tumblagooda Sandstone (Member A)	Quartzarenite with minor claystone
987.8568	0.11	0.14	0.12	0.12			0.1225		

988.1616	0.08	0.07	0.07	0.07		0.0725		
988.4664	0.01	0.02	0.02	0.03		0.02		
988.7712	0.05	0.04	0.04			0.043333333		
989.076	0.09	0.1	0.09	0.1		0.095		
989.3808	0.05	0.06	0.06	0.04		0.0525		
989.6856	0.06	0.06	0.05	0.06		0.0575		
989.9904	0.1	0.11	0.11	0.1		0.105		
990.2952	0.13	0.13	0.13			0.13		
990.6	0.27	0.27	0.29	0.25		0.27		
990.9048	0.03	0.03	0.03			0.03		
1349.654	0.05	0.05	0.05			0.05	Tumblagooda Sandstone (Member A)	Quartzarenite with minor claystone
1349.959	0.03	0.03	0.04	0.03		0.0325		
1350.264	0.03	0.03	0.02	0.04		0.03		
1350.569	0.03	0.04	0.05	0.03		0.0375		
1350.874	0.04	0.04	0.05			0.043333333		
1351.178	0.04	0.04	0.03			0.036666667		
1351.483	0.03	0.03	0.03			0.03		
1351.788	0.03	0.03	0.03			0.03		
1352.093	0.02	0.04	0.05	0.04	0.05	0.04		
1352.398	0.04	0.04	0.04	0.05		0.0425		
1352.702	0.04	0.04	0.03	0.04		0.0375		

Gun Island 1								
DEPTH (m)	**1**	**2**	**3**	**4**	**5**	**6**	**AVERAGE (SI)**	**SEQUENCE**	**ROCK TYPE**
135.9408	0.02	0.04	0.05	0.05			0.04	Yaragadee	Sandstone with minor coal, shale and siltstone
136.2456	0.06	0.05	0.05				0.053333333		
136.5504	0.04	0.04	0.04				0.04		
136.8552	0.04	0.05	0.05				0.046666667		
137.16	0.04	0.03	0.04				0.036666667		

137.4648	0.03	0.02	0.04			0.03		
137.7696	0.02	0.02	0.05	0.02		0.0275		
138.0744	0.04	0.04	0.04			0.04		
138.3792	0.05	0.05	0.04			0.046666667		
138.684	0.01	0.02	0.02			0.016666667		
308.1528	0.05	0.06	0.05			0.053333333	Yaragadee	Sandstone with minor coal, shale and siltstone
308.4576	0.04	0.05	0.05	0.06		0.05		
308.7624	0.05	0.05	0.05			0.05		
309.0672	0.05	0.06	0.05			0.053333333		
309.372	0.04	0.05	0.04			0.043333333		
309.6768	0.05	0.06	0.06			0.056666667		
309.9816	0.07	0.07	0.07			0.07		
310.2864	0.06	0.06	0.06			0.06		
310.5912	0.04	0.06	0.05	0.04		0.0475		
310.896	0.06	0.05	0.06	0.05		0.055		
311.5056	0.06	0.06	0.05	0.05		0.055		
312.1152	0.04	0.03	0.04			0.036666667		
766.8768	0.09	0.1	0.09			0.093333333	Yaragadee	Sandstone with minor coal, shale and siltstone
767.1816	0.1	0.1	0.1			0.1		
767.4864	0.08	0.06	0.08	0.08		0.075		
918.972	0.07	0.06	0.08			0.07	Yaragadee	Sandstone with minor coal, shale and siltstone
919.5816	0.03	0.05	0.04	0.07		0.0475		
920.1912	0.09	0.07	0.06	0.08		0.075		
920.8008	0.07	0.07	0.09	0.08		0.0775		
921.4104	0.07	0.09	0.08	0.09	0.08	0.082		
922.02	0.07	0.07	0.05	0.05		0.06		

1050.95	0.05	0.07	0.06	0.06	0.06	Yaragadee	Sandstone with minor coal, shale and siltstone
1051.56	0.04	0.05	0.04		0.043333333		
1052.17	0.09	0.08	0.09		0.086666667		
1052.779	0.1	0.08	0.08	0.08	0.085		
1053.389	0.13	0.15	0.13	0.14	0.1375		
1053.998	0.12	0.12	0.11	0.11	0.115		
1054.608	0.06	0.07	0.06		0.063333333		
1055.218	0.06	0.04	0.05	0.05	0.05		
1055.827	0.05	0.05	0.05		0.05		
1056.437	0.07	0.06	0.07		0.066666667		
1057.046	0.06	0.07	0.06		0.063333333		
1156.716	0.08	0.08	0.05	0.05	0.065	Yaragadee	Sandstone with minor coal, shale and siltstone
1157.326	0.08	0.08	0.07	0.07	0.075		
1157.935	0.06	0.05	0.08	0.07	0.065		
1158.545	0.14	0.14	0.13	0.12	0.1325		
1360.018	0.05	0.05	0.05		0.05	Yaragadee	Sandstone with minor coal, shale and siltstone
1360.627	0.06	0.06	0.07	0.06	0.0625		
1515.466	0.19	0.19	0.18	0.16	0.18	Yaragadee	Sandstone with minor coal, shale and siltstone
1516.075	0.04	0.04	0.04	0.04	0.04		
1516.685	0.11	0.11	0.13	0.11	0.115		
1517.294	0.19	0.18	0.16	0.16	0.1725		
1517.904	0.14	0.17	0.17	0.17	0.1625		

1704.746	0.13	0.13	0.12	0.12	0.125	Yaragadee	Sandstone with minor coal, shale and siltstone
1705.356	0.1	0.12	0.12	0.13	0.1175		
1705.966	0.14	0.15	0.15	0.15	0.1475		
1706.575	0.32	0.32	0.31	0.31	0.315		
1707.185	0.16	0.15	0.14	0.14	0.1475		
1707.794	0.13	0.12	0.12	0.12	0.1225		
1708.404	0.14	0.13	0.12	0.12	0.1275		
1709.014	0.14	0.15	0.15	0.15	0.1475		
1709.623	0.12	0.12	0.11	0.11	0.115		
1710.233	0.11	0.11	0.11	0.11	0.11		
1859.28	0.21	0.2	0.21	0.21	0.2075	Yaragadee	Sandstone with minor coal, shale and siltstone
1859.89	0.14	0.12	0.13	0.13	0.13		
1860.499	0.17	0.17	0.17	0.16	0.1675		
1861.109	0.13	0.14	0.13	0.13	0.1325		
1861.718	0.19	0.19	0.21	0.2	0.1975		
1862.328	0.22	0.22	0.23	0.22	0.2225		
2044.294	0.18	0.16	0.16	0.18	0.17	Yaragadee	Sandstone with minor coal, shale and siltstone
2044.903	0.09	0.1	0.11	0.1	0.1		
2045.513	0.15	0.15	0.14	0.14	0.145		
2046.122	0.17	0.17	0.17	0.15	0.165		
2046.732	0.26	0.29	0.25	0.27	0.2675		
2188.769	0.17	0.16	0.17	0.16	0.165	Cadda	Sandstone with minor siltstone and shale
2189.378	0.19	0.18	0.17	0.18	0.18		
2189.988	0.14	0.15	0.17	0.15	0.1525		
2190.598	0.19	0.18	0.17	0.18	0.18		

2191.207	0.23	0.23	0.23	0.22		0.2275		
2357.018	0.18	0.18	0.17	0.17		0.175	Cadda	Sandstone with minor siltstone and shale
2357.628	0.14	0.16	0.14	0.13		0.1425		
2358.238	0.21	0.21	0.21	0.22		0.2125		
2358.847	1.03	1.18	1.24	1.18	1.08	1.142		
2520.696	0.09	0.1	0.08	0.09		0.09	Cattamarra	Sandstone and sandy carbonaceous limestone
2521.306	0.12	0.12	0.11	0.1		0.1125		
2521.915	0.18	0.19	0.2	0.15		0.18		
2522.525	0.09	0.1	0.09	0.07		0.0875		
2523.134	0.12	0.13	0.14	0.14		0.1325		
2660.904	0.18	0.18	0.18	0.17		0.1775	Cattamarra	Sandstone and sandy carbonaceous limestone
2661.514	0.16	0.15	0.14	0.16		0.1525		
2662.123	0.18	0.19	0.18	0.17		0.18		
3250.387	0.17	0.17	0.14	0.16		0.16	Eneabba	Sandstone with minor gravel, claystone and siltstone
3250.997	0.3	0.28	0.29	0.29		0.29		
3251.606	0.12	0.13	0.1	0.11		0.115		
3252.216	0.07	0.09	0.08	0.09		0.0825		
3252.826	0.19	0.19	0.18	0.2		0.19		
3365.297	0.05	0.05	0.04	0.06		0.05	Eneabba	Sandstone with minor gravel, claystone and siltstone
3365.906	0.06	0.07	0.05	0.06		0.06		
3366.516	0.09	0.09	0.1	0.08		0.09		
3367.126	0.06	0.05	0.05	0.05		0.0525		

3367.735	0.07	0.06	0.07	0.06		0.065		
3599.383	0.21	0.2	0.2	0.21		0.205	Eneabba	Sandstone with minor gravel, claystone and siltstone
3599.993	0.15	0.14	0.12	0.14		0.1375		
3600.602	0.22	0.23	0.22	0.2		0.2175		
3601.212	0.18	0.19	0.23	0.2		0.2		
3601.822	0.24	0.25	0.23	0.26		0.245		
3721.913	0.2	0.18	0.17	0.17		0.18	Eneabba	Sandstone with minor gravel, claystone and siltstone
3722.522	0.2	0.16	0.2	0.19		0.1875		
3723.132	0.22	0.21	0.21	0.2		0.21		
3723.742	0.24	0.21	0.21	0.21		0.2175		

Houtman 1								
DEPTH (m)	**1**	**2**	**3**	**4**	**5**	**6**	**AVERAGE (SI)**	**SEQUENCE**	**ROCK TYPE**
3073	0.11	0.14	0.14	0.13			0.13	Cadda	Sandstone with minor siltstone and shale
3073.5	0.14	0.12	0.13	0.13			0.13		
3074	0.12	0.12	0.11				0.116666667		
3074.5	0.11	0.14	0.12	0.13	0.12		0.124		
3075	0.08	0.07	0.08	0.08			0.0775		
3075.5	0.09	0.1	0.1	0.1			0.0975		
3076	0.13	0.12	0.12	0.13			0.125		
3076.5	0.14	0.14	0.12	0.15			0.1375		
3077	0.14	0.11	0.11	0.11			0.1175		
3077.5	0.13	0.13	0.12				0.126666667		
3078	0.11	0.11	0.1				0.106666667		
3078.5	0.23	0.24	0.24	0.23			0.235		
3079	0.22	0.2	0.23	0.21			0.215		
3079.5	0.2	0.2	0.21				0.203333333		

3080	0.19	0.19	0.2	0.2			0.195		
3080.5	0.22	0.21	0.2				0.21		
3081	0.14	0.16	0.15	0.17			0.155		
3081.5	0.17	0.17	0.17				0.17		
3082	0.15	0.14	0.13	0.14			0.14		
3082.5	0.13	0.12	0.15	0.16	0.13		0.138		
3083	0.18	0.19	0.19				0.186666667		
3083.5	0.16	0.16	0.16				0.16		
3084	0.2	0.19	0.2	0.2			0.1975		
3084.5	0.2	0.2	0.18	0.19			0.1925		
3085	0.21	0.21	0.2				0.206666667		
3158.5	0.09	0.06	0.07	0.11	0.1		0.086	Cadda	Sandstone with minor siltstone and shale
3159	0.18	0.16	0.16	0.16			0.165		
3159.5	0.2	0.18	0.2	0.18			0.19		
3160	0.19	0.19	0.19				0.19		
3160.5	0.21	0.21	0.23	0.21			0.215		
3161	0.18	0.2	0.21	0.21	0.21		0.202		
3161.5	0.17	0.15	0.16	0.17	0.16	0.16	0.161666667		
3162	0.21	0.2	0.18	0.15	0.16	0.16	0.176666667		
3162.5	0.12	0.11	0.12	0.12			0.1175		
3163	0.37	0.35	0.36	0.36			0.36		
3163.5	0.14	0.13	0.14				0.136666667		
3164	0.12	0.12	0.12				0.12		
3164.5	0.11	0.11	0.11				0.11		
3165	0.61	0.64	0.55	1.21	1.22	1.25	0.913333333		Volcanic pebble
3165.5	0.18	0.21	0.19	0.15			0.1825		
3166	0.22	0.21	0.22	0.22			0.2175		
3166.5	0.18	0.17	0.18	0.16			0.1725		
3167	0.19	0.18	0.18				0.183333333		
3167.5	0.19	0.19	0.17	0.2			0.1875		

3168	0.41	0.42	0.32	0.4	0.34	0.35	0.373333333		
3168.5	0.23	0.22	0.24				0.23		
3169	0.22	0.24	0.23				0.23		
3169.5	0.27	0.24	0.23	0.22			0.24		
3170	1.58	1.16	1.55	1.58	1.57		1.488		
3170.5	0.09	0.1	0.12	0.1	0.11		0.104		
3171	0.18	0.19	0.18				0.183333333		
3362	0.07	0.08	0.08				0.076666667	Cadda	Sandstone with minor siltstone and shale
3362.5	0.09	0.09	0.11	0.15	0.14		0.116		
3363	0.07	0.08	0.06	0.08			0.0725		
3363.5	0.09	0.09	0.1	0.08			0.09		
3364	0.09	0.09	0.1				0.093333333		
3364.5	0.16	0.2	0.15	0.17	0.15		0.166		
3365	0.14	0.14	0.14				0.14		
3365.5	0.09	0.08	0.09	0.08			0.085		
3387	0.07	0.09	0.07	0.09			0.08	Cattamarra	Sandstone and sandy carbonaceous limestone
3387.5	0.13	0.14	0.18	0.19			0.16		
3388	0.08	0.08	0.07				0.076666667		
3388.5	0.13	0.13	0.13				0.13		
3389	0.08	0.12	0.09	0.09	0.11	0.1	0.098333333		
3389.5	0.11	0.1	0.09	0.09	0.09		0.096		
3390	0.09	0.11	0.11	0.14	0.12		0.114		
3390.5	0.12	0.1	0.11	0.11			0.11		
3391	0.14	0.14	0.13				0.136666667		
3391.5	0.11	0.1	0.09	0.11			0.1025		
3392	0.06	0.04	0.05	0.05			0.05		
3392.5	0.05	0.06	0.06	0.06			0.0575		
3393	0.08	0.08	0.07	0.08			0.0775		

3393.5	0.11	0.11	0.12	0.13		0.1175
3394	0.15	0.15	0.13	0.13		0.14
3394.5	0.13	0.12	0.1	0.12	0.12	0.118
3395	0.11	0.09	0.12	0.1	0.12	0.108

Jurien 1								
DEPTH (m)	**1**	**2**	**3**	**4**	**5**	**6**	**AVERAGE (SI)**	**SEQUENCE**	**ROCK TYPE**
689.152	0.12	0.08	0.06	0.07	0.07		0.08	Basement	Metamorphic Basement

Sue 1								
DEPTH (m)	**1**	**2**	**3**	**4**	**5**	**6**	**AVERAGE (SI)**	**SEQUENCE**	**ROCK TYPE**
3052.572	0.65	0.62	0.72	0.69	0.76	0.72	0.693333333	Basement	Metamorphic Basement
3073.756	0.09	0.08	0.07	0.09			0.0825		

Appendix 2 – Comparison between depth to Precambrian from wells and power spectra

Well name	Depth to PreCambrian (m)	10 x 10 km			15 x 15 km			20 x 20 km		
		Depth (m)	Difference	Percentage difference	Depth (m)	Difference	Percentage difference	Depth (m)	Difference	Percentage difference
Arramall 1	2188	1876.8	311.2	14.2	1195.8	992.2	45.3	3228.8	-1040.8	-47.6
Arrowsmith 1	3363	3519.4	-156.4	-4.7	3753.6	-390.6	-11.6	3127.9	235.1	7
Beharra 1	2013	2266.5	-253.5	-12.6	1980.9	32.1	1.6	2294.3	-281.3	-14
BMR Beagle Ridge 10A	1454	1795.1	-341.1	-23.5				1674.7	-220.7	-15.2
Bonnifield 1	991				1319.6	-328.6	-33.2	1467.7	-476.7	-48.1
Cadda 1	2661	2690.6	-29.6	-1.1	2987.5	-326.5	-12.3	2562.3	98.7	3.7
Cliff Head 4	1562	1952.4	-390.4	-25	2100.2	-538.2	-34.5			
Cliff Head 5	1473	1897	-424	-28.8	1132.5	340.5	23.1	2271.3	-798.3	-54.2
Dongara 6	1515	1752.3	-237.3	-15.7	1391.7	123.3	8.1	1634.4	-119.4	-7.9
Gairdner 1	1990				2517	-527	-26.5	2055.3	-65.3	-3.3
Jurien 1	965	1064.1	-99.1	-10.3	1644.6	-679.6	-70.4	1254	-289	-29.9
Mentelle 1	1477	1237.3	239.7	16.2	2042.7	-565.7	-38.3	1907.1	-430.1	-29.1
Rakrani 1	1189				934.5	254.5	21.4	1198.4	-9.4	-0.8
Robb 1	1940	2237.2	-297.2	-15.3	2350.2	-410.2	-21.1	1879.6	60.4	3.1
Twin Lions 1	1513	2411.6	-898.6	-59.4	1095.5	417.5	27.6	1883.9	-370.9	-24.5
Wattle Grove 1	762				1052.7	-290.7	-38.1	1082.4	-320.4	-42
Wendy 1	1390	1227.1	162.9	11.7	1608.7	-218.7	-15.7	1277.6	112.4	8.1
Woodada 19	2795				2725.9	69.1	2.6	2500.3	294.7	10.5
Woolmulla 1	2652	2624.1	27.9	1.1	2582.9	69.1	2.6	3351.4	-699.4	-26.4
	Average			-10.9			-9.4			-17.3

Well name	Depth to PreCambrian (m)	30 x 30 km Depth (m)	30 x 30 km Difference	30 x 30 km Percentage difference	40 x 40 km Depth (m)	40 x 40 km Difference	40 x 40 km Percentage difference	50 x 50 km Depth (m)	50 x 50 km Difference	50 x 50 km Percentage difference
Arramall 1	2188	1289.8	898.2	41.1	3224.6	-1036.6	-47.4	2206.3	-18.3	-0.8
Arrowsmith 1	3363	2777.1	585.9	17.4	3029.4	333.6	9.9	2924.9	438.1	13
Beharra 1	2013	1793.5	219.5	10.9	2454.4	-441.4	-21.9	2917.5	-904.5	-44.9
BMR Beagle Ridge 10A	1454	1805.6	-351.6	-24.2						
Bonnifield 1	991	978.9	12.1	1.2	1015.5	-24.5	-2.5			
Cadda 1	2661				2969.3	-308.3	-11.6	2700.4	-39.4	-1.5
Cliff Head 4	1562	1905.7	-343.7	-343.7	1860.6	-298.6	-19.1	3123.3	-1561.3	-100
Cliff Head 5	1473	2179.8	-706.8	-48	1393.7	79.3	5.4	1720.8	-247.8	-16.8
Dongara 6	1515	1323.4	191.6	12.6	1832.1	-317.1	-20.9	1595.6	-80.6	-5.3
Gairdner 1	1990				2118.9	-128.9	-6.5	1353.4	636.6	32
Jurien 1	965	1658.5	-693.5	-71.9						
Mentelle 1	1477	1912	-435	-29.4						
Rakrani 1	1189	1376.3	-187.3	-15.8	1539.5	-350.5	-29.5	1581.8	-392.8	-33
Robb 1	1940							2885.2	-945.2	-48.7
Twin Lions 1	1513	2131.9	-618.9	-40.9						
Wattle Grove 1	762	822.8	-60.8	-8				973.5	-211.5	-27.8
Wendy 1	1390				1386.2	3.8	0.3	1318.7	71.3	5.1
Woodada 19	2795	2570	225	8	2166.8	628.2	22.5	2674.6	120.4	4.3
Woolmulla 1	2652							2073.7	578.3	21.8
	Average			-35.1			-10.1			-14.5

Well name	Depth to PreCambrian (m)	60 x 60 km		
		Depth (m)	Difference	Percentage difference
Arramall 1	2188	2266.3	-78.3	-3.6
Arrowsmith 1	3363	2239.9	1123.1	33.4
Beharra 1	2013			
BMR Beagle Ridge 10A	1454			
Bonnifield 1	991	1098.3	-107.3	-10.8
Cadda 1	2661	2309.8	351.2	13.2
Cliff Head 4	1562	1436.2	125.8	8.1
Cliff Head 5	1473	2211.1	-738.1	-50.1
Dongara 6	1515	1337.6	177.4	11.7
Gairdner 1	1990	2122.4	-132.4	-6.7
Jurien 1	965			
Mentelle 1	1477			
Rakrani 1	1189	1537.8	-348.8	-29.3
Robb 1	1940	1866.8	73.2	3.8
Twin Lions 1	1513			
Wattle Grove 1	762	1329.7	-567.7	-74.5
Wendy 1	1390	1264.3	125.7	9
Woodada 19	2795	3298.2	-503.2	-18
Woolmulla 1	2652			
	Average			-8.8